

New Herbig–Haro objects and giant outflows in Orion

S. L. Mader,¹ W. J. Zealey,¹ Q. A. Parker² and M. R. W. Masheder^{3,4}

¹*Department of Engineering Physics, University of Wollongong, Northfields Avenue, Wollongong, NSW 2522, Australia*

²*Anglo-Australian Observatory, Coonabarabran, NSW 2357, Australia*

³*Department of Physics, University of Bristol, Bristol BS8 1TL*

⁴*Netherlands Foundation for Research in Astronomy, PO Box 2, 7900 AA Dwingeloo, the Netherlands*

Accepted 1999 June 29. Received 1999 May 11; in original form 1998 June 25

ABSTRACT

We present the results of a photographic and CCD imaging survey for Herbig–Haro (HH) objects in the L1630 and L1641 giant molecular clouds in Orion. The new HH flows were initially identified from a deep H α film from the recently commissioned AAO/UKST H α Survey of the southern sky. Our scanned H α and broad-band *R* images highlight both the improved resolution of the H α survey and the excellent contrast of the H α flux with respect to the broad-band *R*. Comparative IVN survey images allow us to distinguish between emission and reflection nebulosity. Our CCD H α , [S II], continuum and *I*-band images confirm the presence of a parsec-scale HH flow associated with the Ori I-2 cometary globule, and several parsec-scale strings of HH emission centred on the L1641-N infrared cluster. Several smaller outflows display one-sided jets. Our results indicate that, for declinations south of -6° in L1641, parsec-scale flows appear to be the major force in the large-scale movement of optical dust and molecular gas.

Key words: surveys – stars: formation – ISM: individual: L1630 – ISM: individual: L1641 – ISM: jets and outflows.

1 INTRODUCTION

The process of star formation is a highly disruptive event in which both infall and outflow of material occur simultaneously in the production of a protostellar core. The outflow phase is characterized by the impact of high-velocity winds with the surrounding interstellar medium, which manifest as bipolar molecular outflows, Herbig–Haro (HH) objects and jets. Multi-wavelength observations have shown HH objects and jets to be regions of shock-excited gas emitting H α ($\lambda 6563$), [O I] ($\lambda \lambda 6300, 6363$) and [S II] ($\lambda \lambda 6716, 6731$) in the visible and H $_2$ ($2.12 \mu\text{m}$) in the infrared. Their energy sources range from deeply embedded protostars to optical T Tauri and Herbig Ae/Be stars.

With the introduction of large-format CCD detectors, wide-field imaging has shown that HH flows are more abundant and an order of magnitude larger than previously thought. Recent narrow-band imaging of the NGC 1333 star-forming region (SFR) by Bally, Devine & Reipurth (1996) found a high concentration of HH objects within a $1/4 \text{ deg}^2$ region. A similar result was found by Yun, Bally & Devine (1997) who conducted a near-infrared H $_2$ ($2.12 \mu\text{m}$) survey of the OMC-2 and OMC-3 regions in Orion. Based on well-studied flows such as HH 1/2, HH 34 and HH 46/47, it was generally thought that their extent ($\sim 0.3 \text{ pc}$) was typical of outflows from low-mass stars. Bally & Devine (1994) were the first to question this view with their suggestion that the HH 34 flow in Orion is actually 3 pc in extent. Their idea was confirmed

with deep CCD imaging and proper motion studies of individual knots (Devine et al. 1997). To date, around 20 giant ($>1 \text{ pc}$) HH flows have been associated with low-mass stars (Eisloffel & Mundt 1997; Reipurth, Bally & Devine 1997).

A large number of giant HH flows (and their small-scale counterparts) may have dramatic effects on the stability and chemical composition of a giant molecular cloud (GMC). It has been suggested that outflows may provide a mechanism for self-regulated star formation and large-scale bulk motions within GMCs (Foster & Boss 1996). It is therefore important to gain information on the distribution of outflows and particularly giant flows within SFRs. The new Anglo-Australian Observatory (AAO) and United Kingdom Schmidt Telescope (UKST) H α Survey of the southern Galactic plane (Parker & Phillipps 1998a) will be beneficial for such studies, as it provides an unbiased search for new HH objects over entire SFRs with its wide-field and high-resolution capabilities.

In this paper we concentrate on a search for new HH objects in the first, deep H α film of the Orion SFR. The distance to the Orion region lies between 320 and 500 pc (Brown, De Geus & De Zeeuw 1994). Here we adopt a distance of 470 pc based on known HH objects in the region (Reipurth, in preparation). Strong emission and reflection nebulosity in the region makes searching for HH objects difficult. Previous attempts at surveys for faint red nebulosities in L1630 and L1641 have used standard broad-band IIIaF *R* plates (IIIaF emulsion and RG630 filter), which were

limited to subregions clear of high background emission (Reipurth 1985; Malin, Ogura & Walsh 1987; Reipurth & Graham 1988; Ogura & Walsh 1991). The new, deep fine-resolution $H\alpha$ films enable us to conduct a more complete survey for emission-line nebulosities for consequent follow-up observations.

In Section 2 we present a brief introduction to the specifics of the $H\alpha$ survey and details on observations and data reduction. Results are presented in Section 3 where individual objects are discussed. In Section 4 we make some general conclusions and references to future work.

2 OBSERVATIONS AND DATA REDUCTION

2.1 The AAO/UKST $H\alpha$ Survey

Under the auspices of the AAO, the UKST has recently embarked on a new $H\alpha$ survey of the southern Galactic plane, Magellanic Clouds and selected regions. No systematic high-resolution $H\alpha$ survey has been carried out in the southern hemisphere since the pioneering work of Gum (1955) and Rodgers, Campbell & Whiteoak (1960). With the increase in resolution and sensitivity of differing wavelength technologies, there has been the need to perform an $H\alpha$ survey with similar attributes.

The unusually large, single-element $H\alpha$ interference filter is centred on 6590 Å with a bandpass of 70 Å. It is probably the largest filter of its type in use in astronomy. Coated on to a full-field 356 × 356 mm² RG610 glass substrate, the 305-mm clear circular aperture provides a 5°.5 field of view. Further details of the filter properties and specifications are given by Parker & Bland-Hawthorn (1998). The detector is the fine-grained, high-resolution Kodak Tech Pan film which has been the emulsion of choice at the UKST for the last 4 years. This is due to its excellent imaging, low noise and high Detector Quantum Efficiency (DQE) (e.g. Parker, Phillipps & Morgan 1995; Parker et al., in preparation). Tech Pan also has a useful sensitivity peak at $H\alpha$ as it was originally developed for solar patrol work. Although electronic devices such as CCDs are the preferred detector in much of modern astronomy, they cannot yet match the fine resolution and wide-field coverage of the Tech Pan film and UKST combination.

Typical deep $H\alpha$ exposures are of 3-h duration, a compromise between depth, image quality and survey progress as the films are still not sky-limited after this time. The southern Galactic plane survey requires 233 fields on 4° centres and will take 3 years to complete. Initial survey test exposures have demonstrated that the combination of high-quality interference filter and Tech Pan film is far superior, for the detection and resolution of faint emission features near the sky background, to any previous combination of filter and photographic plate used for narrow-band observations (Parker & Phillipps 1998a). It is the intention that the original films will be digitized using the Royal Observatory Edinburgh SuperCOSMOS facility (Miller et al. 1992). It is planned to

release a calibrated atlas of digital data to the wider astronomical community as soon as possible.

2.2 Photographic astrometry and image reduction

For the Orion region, a deep 3-h $H\alpha$ exposure was obtained on 1997 December 2 during a period of good seeing. The plate (HA 17828) was centred at 05^h36^m, −04°00′ (1950) and designated grade A based on standard UKST visual quality control procedures by resident UKST staff. Three independent visual scans of the film were carefully made by QAP, SLM and WJZ using an eyepiece and later a 10× binocular microscope. HH objects display a wide range of morphologies including knots, arcs and jets. A combined list of such features was produced and served as the basis for subsequent astrometry. The new $H\alpha$ images were then compared with deep non-survey UKST IIIaJ, IIIaF and IVN broad-band copy plates of the same field to confirm the objects as true emission-line sources. The plates used and their characteristics are presented in Table 1.

Crude positions for each object were first determined using simple XY positions from the film and transformed to B1950 coordinates by use of the UKST program PLADAT. Accurate positions were then obtained by using SkyView FITS files of the surrounding region. This resulted in a positional accuracy within 2 arcsec for each object. Digitized images of each source were then made using a video digitizing system (Zealey & Mader 1997, 1998). This enabled us to process images via unsharp masking and histogram enhancement to recover the original detail as seen on the Tech Pan film.

2.3 CCD observations

2.3.1 Optical

As the Orion region shows highly structured background emission, it is important that we distinguish between photoionised filamentary structures and bona fide HH objects. This can be accomplished with $H\alpha$ and [S II] images by noting that HH objects usually have [S II]/ $H\alpha$ ratios >1 compared with [S II]/ $H\alpha$ <1 for emission associated with H II regions. We obtained narrow- and broad-band images of HH candidates at the Australian National University 1.0-m telescope at Siding Spring Observatory during various periods in 1998 January–April. Imaging was done with a 2048 × 2048 TEK CCD mounted at the $f/8$ Cassegrain focus. The 0.6-arcsec pixels gave a field of view of 20.48 × 20.48 arcmin². The seeing during usable time was typically <3 arcsec. Narrow-band filters used were [O III] (λ 5016; $\Delta\lambda$ 25 Å), $H\alpha$ (λ 6565; $\Delta\lambda$ 15 Å), [S II] (λ 6732; $\Delta\lambda$ 25 Å) and red continuum (λ 6676; $\Delta\lambda$ 55 Å). The $H\alpha$ filter also transmits the [N II] (λ 6548/6584) lines. We used a standard Kron–Cousins filter for the I -band observations.

Table 1. Plates used in the current survey.

Plate	α_{1950}	δ_{1950}	Date	Emulsion	Filter	Exp (min)	Grade
R 3816	05 ^h 32 ^m	−04°00′	77-12-11	IIIaF	RG630	90	a
J 3828	05 ^h 32 ^m	−04°00′	77-12-16	IIIaJ	GG395	70	a
I 3869	05 ^h 32 ^m	−04°00′	78-01-13	IVN	RG715	60	b
HA 17828	05 ^h 36 ^m	−04°00′	97-12-02	4415	HA659	180	a
R 7462	05 ^h 36 ^m	−09°00′	82-01-26	IIIaF	RG630	90	bI
J 8235	05 ^h 36 ^m	−09°00′	82-11-14	IIIaJ	GG395	65	aT
I 7406	05 ^h 36 ^m	−09°00′	81-12-19	IVN	RG715	90	bI

Typical exposure times were 300 and 900 s for broad- and narrow-band frames respectively. Flat-fields were obtained by illuminating the dome with a halogen lamp. All frames were reduced in a similar fashion with IRAF, where 25 median-combined bias frames were subtracted from source frames prior to flat-fielding. Individual source frames were median-combined to produce the final images. In several instances, we were not able to obtain corresponding continuum frames to our CCD H α and [S II] images. As major HH emission lines do not fall within the spectral response curve of the RG715+IVN filter/emulsion combination ($\Delta\lambda = 6900\text{--}9100 \text{ \AA}$), we use photographic IVN images to serve as continuum images where needed.

2.3.2 Near-infrared

In 1993 January several HH complexes (including Ori I-2) were imaged using IRIS, the AAO infrared camera and low-resolution spectrograph. The 128×128 format array has $60\text{-}\mu\text{m}$ pixels which when used in the $f/15$ imaging mode provided a spatial resolution of 1.94 arcsec per pixel and a 4.1×4.1 arcmin² field of view. Each source was observed through a 1 per cent bandpass filter centred on the H $_2v = 1\text{--}0$ S(1) transition at $2.12 \mu\text{m}$. Continuum images were made using a 4 per cent bandpass filter at $2.24 \mu\text{m}$. Individual frames were linearized, flat-fielded against a dome flat and sky-subtracted before being combined and calibrated using the IRIS image reduction package known as YOGI-FIGARO. A mosaic of 12 frames, each 5 min in length, were combined to form the final images.

3 RESULTS

In Table 2 we list new HH objects identified by our narrow-band CCD imaging of candidates identified from the Orion H α plate. Several of the new objects were identified by Reipurth (1985) as candidate HH objects from his ESO *R* film survey of the Orion region. Objects independently discovered by the CCD imaging of Reipurth, Devine & Bally (1998, hereafter R98) are indicated. In addition to brief comments about their nature and location, Table 2 also suggests possible energy sources based on evidence presented.

3.1 New objects in L1630

Our survey region of the southern portion of L1630 is shown in Fig. 1. The rest of the cloud complex extends several degrees to the north-east of the figure. A diffuse shell of H α emission and a network of bright-rimmed cometary globules surround the multiple OB system σ Ori. Ogura & Sugitani (1998) list many of these globules as remnant clouds which may be sites of retarded star formation. The bright H II regions NGC 2024 and IC 434 (which includes the Horsehead nebula) outline an ionization front between the southern portion of L1630 and σ Ori. This ionization front extends towards the open cluster NGC 1981 which approximately marks the division between L1630 and L1641. The positions of the new HH flows in the region are indicated.

3.1.1 HH 289 (Figs 1–3)

Located on the north-western outskirts of IC 434, the bright-rimmed cometary globule Ori I-2 is host to the low-luminosity ($L_{\text{bol}} = 13 L_{\odot}$) *IRAS* source 05355 – 0416, which drives both a bipolar CO and near-infrared molecular hydrogen outflow (Sugitani et al. 1989; Cernicharo et al. 1992; Hodapp 1994). The *IRAS* source is also associated with an H $_2$ O maser (Wouterloot & Walmsley 1986; Codella et al. 1995).

A comparison between our scanned H α and IVN images (Figs 2a and b) identifies a chain of emission-line objects (objects 2–5) extending to the east of the globule. To the west, we see another emission-line feature (object 1) which appears as an extension of faint emission seen in the IVN image. The H α +[S II] images (Figs 3a and b) confirms the presence of an HH flow, designated here as HH 289. In the central part of the globule, our H α +[S II] and H $_2$ images (Figs 3b and c) show two faint [S II] knots (HH 289 A/B) which mirror the position of the H $_2$ emission. With the exception of knot C, all knots appear [S II]-bright. Knots D–F show large arc-like morphologies which open towards the *IRAS* source. This gives the impression of a bubble surrounding the eastern side of the globule which may represent an interface between the outflow and the UV radiation field from ζ Ori, which is 42 arcmin to the east of Ori I-2.

From the distribution of optical and near-infrared emission

Table 2. New Herbig–Haro flows in Orion.

HH	α_{1950}	δ_{1950}	Former designation ^b	Region	Comment	Energy source
289A	05 ^h 35 ^m 32.4 ^s	–01°46′52″		Ori I-2; L1630	large bow shocks	<i>IRAS</i> 05355–0416
292A ^a	05 ^h 34 ^m 30.7 ^s	–06°36′03″		L1641; NGC 1999	one-sided jet?	BE Ori
301 ^a	05 ^h 34 ^m 12.6 ^s	–06°23′06″	Rei 43	L1641; cluster	cup-shaped object	N23? ^c
302 ^a	05 ^h 34 ^m 22.3 ^s	–06°22′31″	Rei 44	L1641; cluster	bright object	N23? ^c
303B ^a	05 ^h 33 ^m 52.7 ^s	–06°21′24″	Rei 36	L1641; cluster	VLA jet	VLA source
304A ^a	05 ^h 34 ^m 10.6 ^s	–06°16′42″	Rei 41	L1641; cluster	working surfaces	HH 304IRS
305F ^a	05 ^h 33 ^m 58.7 ^s	–06°21′31″		L1641; cluster	symmetric group	PR Ori B?
306B ^a	05 ^h 33 ^m 40.9 ^s	–06°10′33″	Rei 34	L1641; cluster	bow shock	VLA source
307A ^a	05 ^h 33 ^m 39.7 ^s	–06°04′46″		L1641; cluster	large bow shocks	VLA source
308A ^a	05 ^h 33 ^m 51.4 ^s	–06°04′42″		L1641; cluster	linear features	VLA source
309A ^a	05 ^h 33 ^m 35.9 ^s	–05°51′29″	Rei 33	L1641; cluster	fragmented	VLA source
403 ^a	05 ^h 34 ^m 36.9 ^s	–05°55′01″		L1641; cluster	fragmented	L1641-N
404 ^a	05 ^h 34 ^m 46.6 ^s	–05°46′14″		L1641; cluster	sickle-shaped	L1641-N
405 ^a	05 ^h 34 ^m 57.7 ^s	–05°45′20″	Rei 46	L1641; NGC 1980	faint	HH 405IRS
406 ^a	05 ^h 35 ^m 11.7 ^s	–05°41′05″		L1641; NGC 1980	diffuse	HH 405IRS
407A	05 ^h 32 ^m 43.2 ^s	–06°00′32″		L1641; NGC 1980	fragmented	V380 Ori?
444D	05 ^h 37 ^m 18.6 ^s	–02°31′52″		IC 434; L1630	one-sided jet	V510 Ori

^aIndependently identified by R98. ^bReipurth (1985). ^cSource in list of Chen et al. (1993).

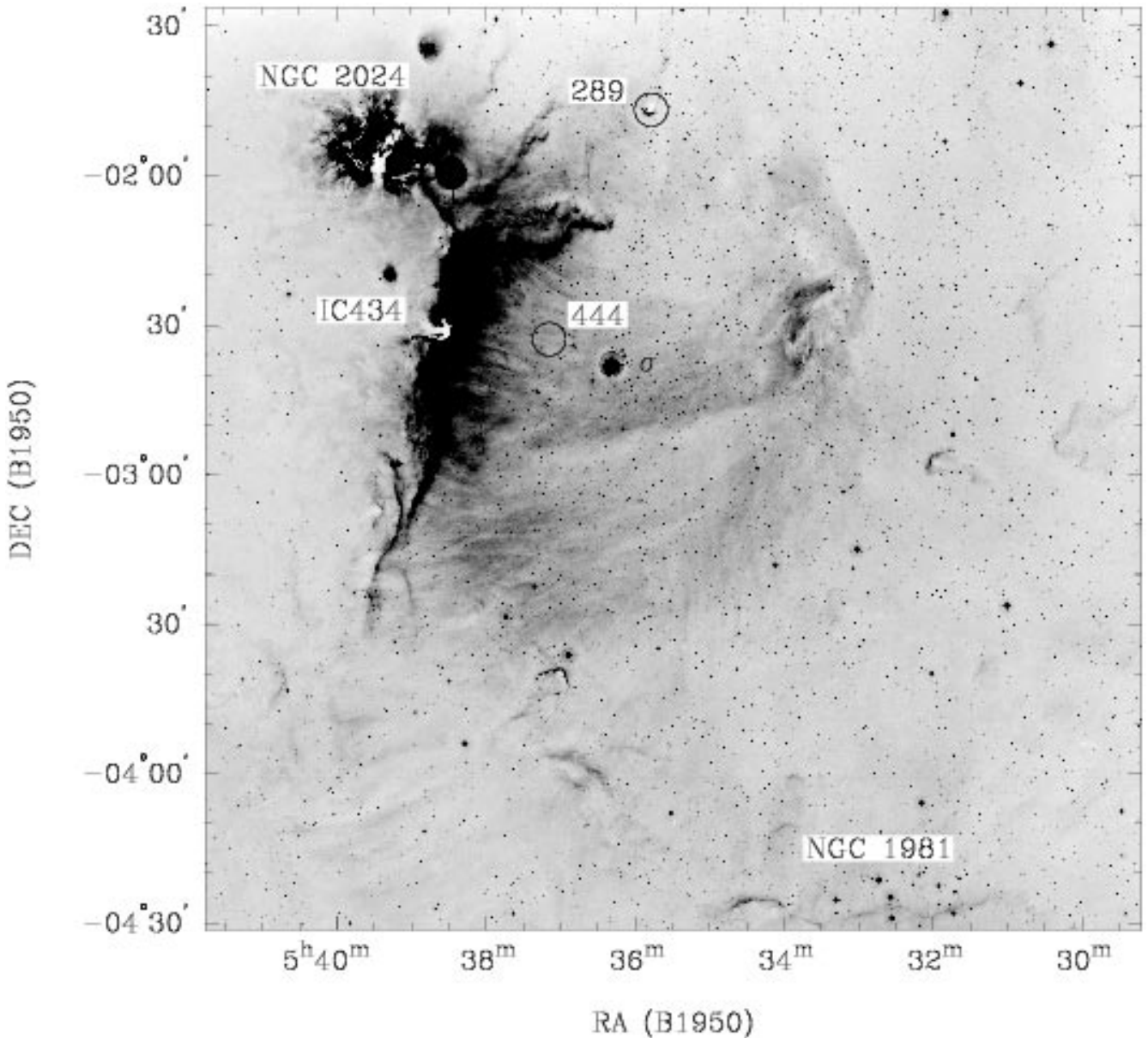


Figure 1. The L1630 survey region. The image was derived from an unsharp-mask print of the $H\alpha$ plate. The upper north-east of the image shows the IC 434 and NGC 2024 $H\text{II}$ regions. Surrounding the σ Ori OB system is a diffuse shell of $H\alpha$ emission in addition to numerous cometary globules and ionization fronts which extend from NGC 2024 to the open cluster NGC 1981. The locations of new HH flows are indicated by their numbers. North is up and east is left in all images.

about the *IRAS* source (Figs 3b and c), we suggest that it is the driving source of the HH 289 outflow. The chain extends 551 arcsec from the *IRAS* source, making the lobe 1.23 pc in projection. This puts the Ori I-2 flow in the class of parsec-scale flows from low-mass stars (Reipurth et al. 1997). As HH objects typically display tangential velocities of the order of 150 km s^{-1} (i.e. Mundt 1988), the age span of the optical knots ranges from 530 yr (knot A) to 8100 yr (knot F). The projected lengths of the (redshifted) CO, H_2 and optical HH flows are 40 arcsec (0.09 pc), 80 arcsec (0.18 pc) and 551 arcsec (1.23 pc) respectively. Apart from knot A, we do not see any evidence of HH emission associated with the blueshifted CO lobe, which we expect will be very faint due to the tenuous medium on the western side of the globule. Deeper $[\text{S II}]$, $[\text{O II}]$ and/or $[\text{O III}]$ images of the western side of the globule may reveal fainter emission.

In Fig. 3(b), we note the appearance of a tube-like feature extending out of the western side of the globule (object 1 in Fig. 2a). It is well aligned and mirrors the inner $[\text{S II}]$ and H_2 knots with respect to the *IRAS* source. As this feature is visible on our Schmidt images, the emission is most probably scattered light reflected off the walls of the cavity formed by the outflow as it bores its way out of the globule. Using AAO/UKST $H\alpha$ material, we have identified a similar feature associated with the cometary globule and outflow complex CG 30/HH 120 (Zealey et al., in preparation). The $H\alpha$ streamer extends to the south-west of the globule and appears to be the optical counterpart of an extensive H_2 filament associated with the infrared source CG 30-IRS1. The tube-like feature in Ori I-2 and the streamer in CG 30 may represent limb-brightened cavities.

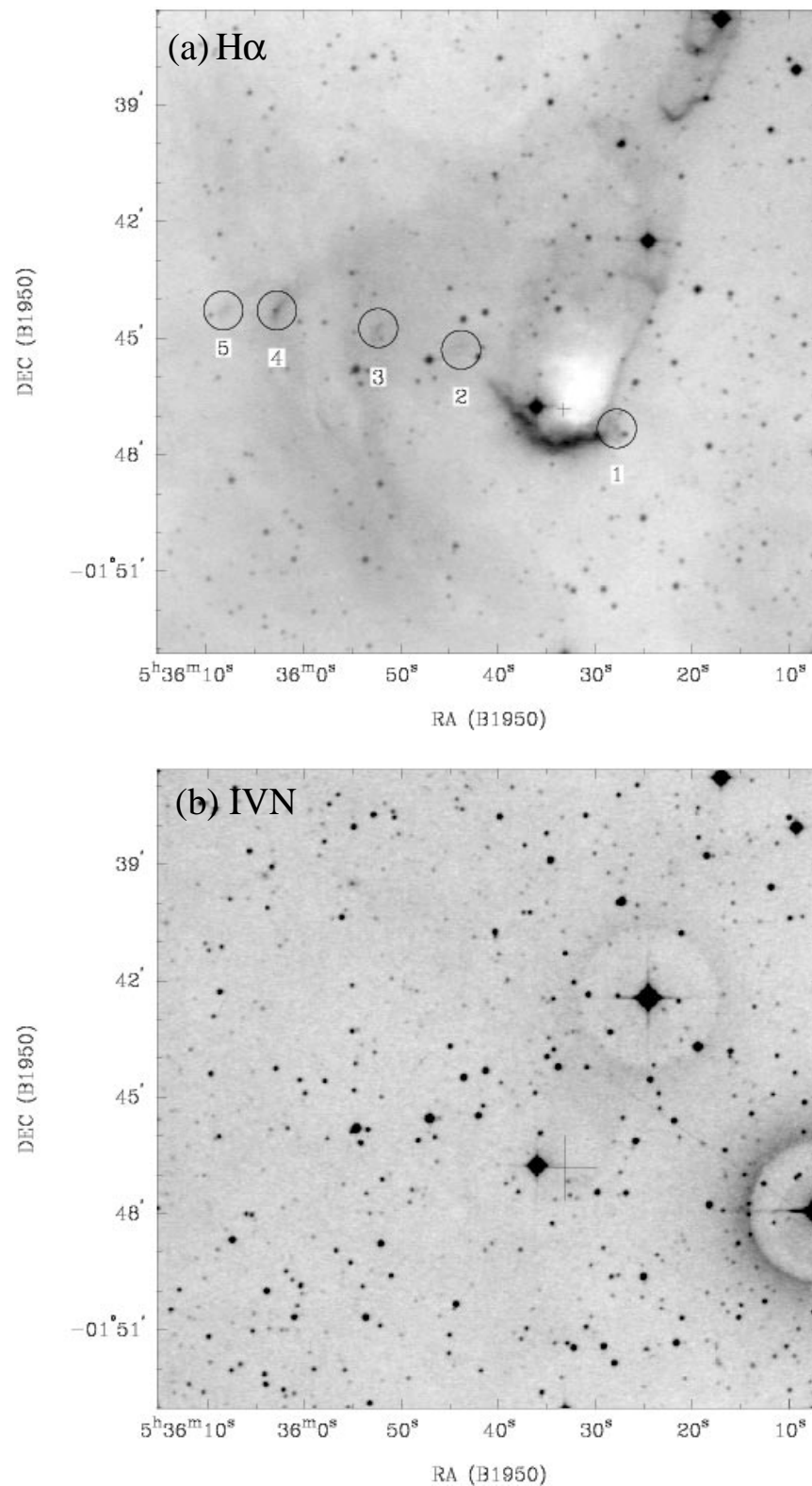


Figure 2. Scanned (a) H α and (b) IVN images of the HH 289 outflow in the Ori I-2 cometary globule. The chain of emission-line objects (1–5) is shown with respect to the embedded IRAS source (cross). Note the bubble-like structure surrounding the eastern side of the globule (see text for details).

3.1.2 HH 444 (Figs 1 and 4)

Located in the vicinity of σ Ori (Fig. 1), V510 Ori (= HBC 177) was first classified as a T Tauri star based on an objective-prism

survey of the Orion region by Sanduleak (1971). Cohen & Kuhi (1979) list the star as a classical T Tauri star (cTTs) with H α equivalent width, $W(\text{H}\alpha)$, < 1 . The H α emission-line survey of Wiramihardja et al. (1991) found the source to be a strong H α

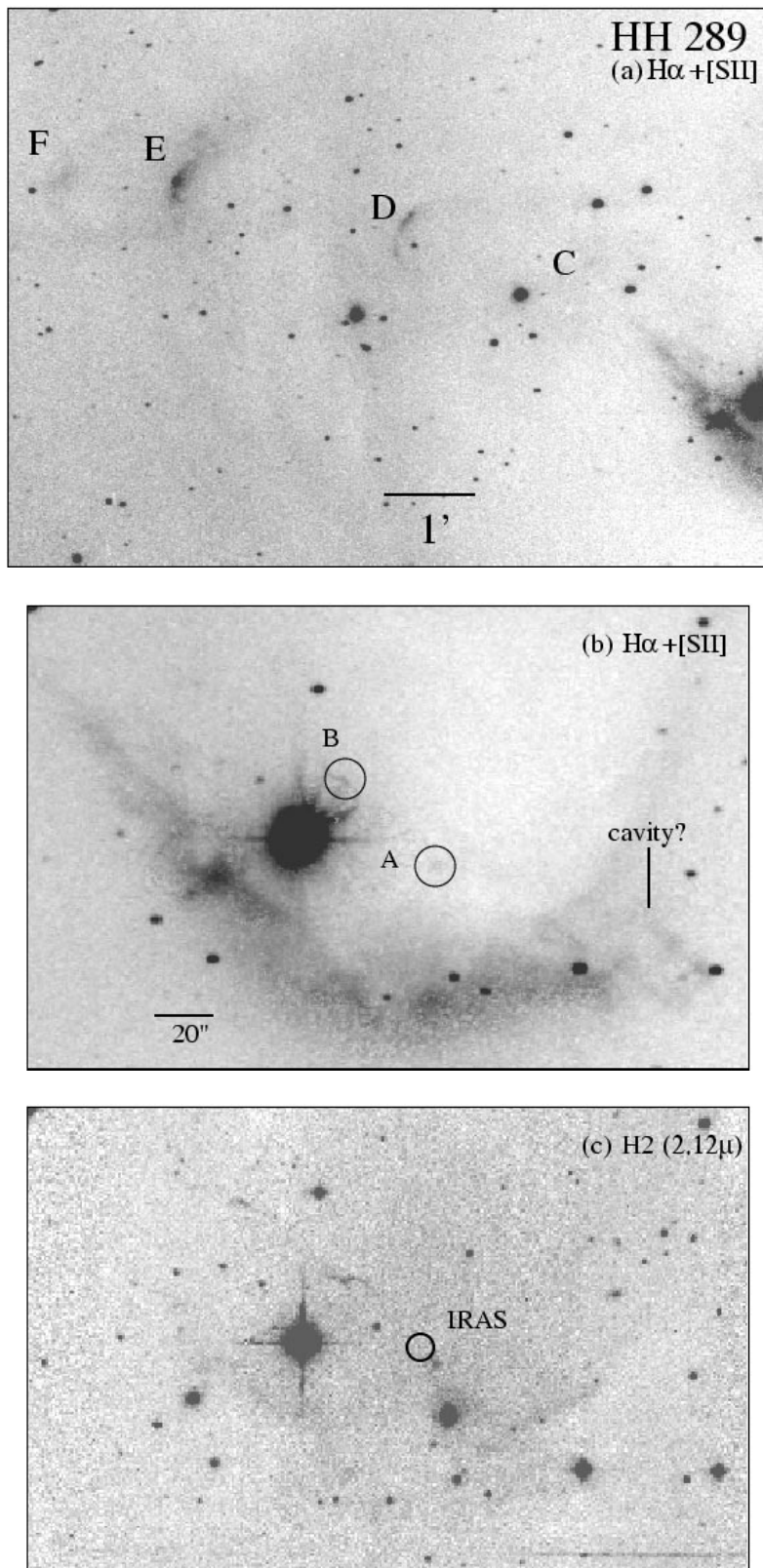


Figure 3. (a) Combined $H\alpha + [S II]$ image of the HH 289 outflow showing the outer knots C–F. The inner region of the globule seen in (b) $H\alpha + [S II]$ and (c) H_2 clearly shows that knots A and B have both optical and near-infrared emission. The position of the *IRAS* source is marked by the circle in the H_2 image. The feature marked ‘cavity?’ may represent a cavity evacuated by the outflow as it propagates out of the globule.

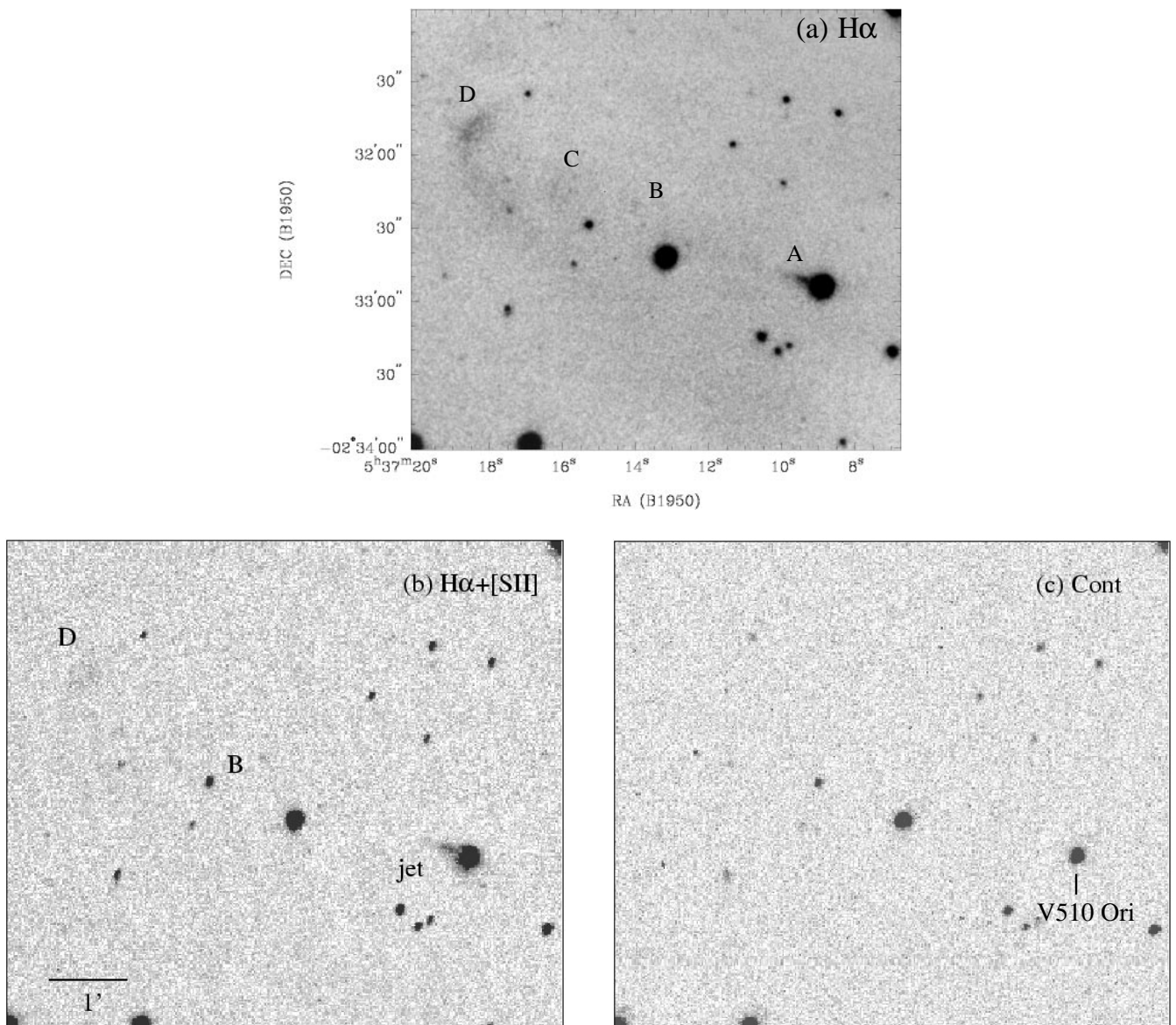


Figure 4. (a) Scanned H α , (b) H α + [S II] and (c) continuum images of the HH 444 outflow. The H α and H α + [S II] images clearly show the jet from V510 Ori. The large bow shock structure, HH 444D, sweeps back towards V510 Ori. Note the absence of a counterjet to the south-west.

emitter with $V = 14.6$ mag as opposed to $V = 13.54$ mag found by Mundt & Bastian (1980).

By use of H α material, the first optical detection of the V510 Ori jet (Parker & Phillipps 1998b; this paper) is shown in Fig. 4(a). The jet has previously been identified by long-slit spectroscopic studies (Jankovics, Appenzeller & Krautter 1983; Hirth, Mundt & Solf 1997). The scanned H α image (Fig. 4a) reveals a highly collimated jet. Several faint knots (A–C) are located 57, 84 and 194 arcsec from V510 Ori. The flow terminates at the large bow shock structure HH 444D, which displays wide wings which sweep back towards the position of V510 Ori.

The H α + [S II] image (Fig. 4b) clearly identifies the HH 444 jet extending from V510 Ori. Owing to the seeing conditions at the time (~ 3 arcsec), we can only confirm the presence of knots B and D in the H α + [S II] image. For the continuum frame (Fig. 4c), conditions were slightly better and, based on the scanned H α and continuum image, knots A–C are considered as pure emission-line

features. The jet appears as two separate parts, with the first section appearing as a dense region extending 10 arcsec from V510 Ori, while a second, fainter part extends a further 6 arcsec. This change may represent several individual condensations not resolved by our images. The total projected length of the optical flow is 0.6 pc.

The small separation between V510 Ori and its jet implies that the jet is still active today and, coupled with the fact that we do not see an obvious counter-flow, suggests an evolved case of a one-sided jet (Rodríguez & Reipurth 1994). High-resolution optical and near-infrared studies of the jet and energy source will be beneficial in determining the nature of this unusual outflow complex.

3.2 New objects in L1641

As shown in Fig. 5, the northern border of L1641 is approximated

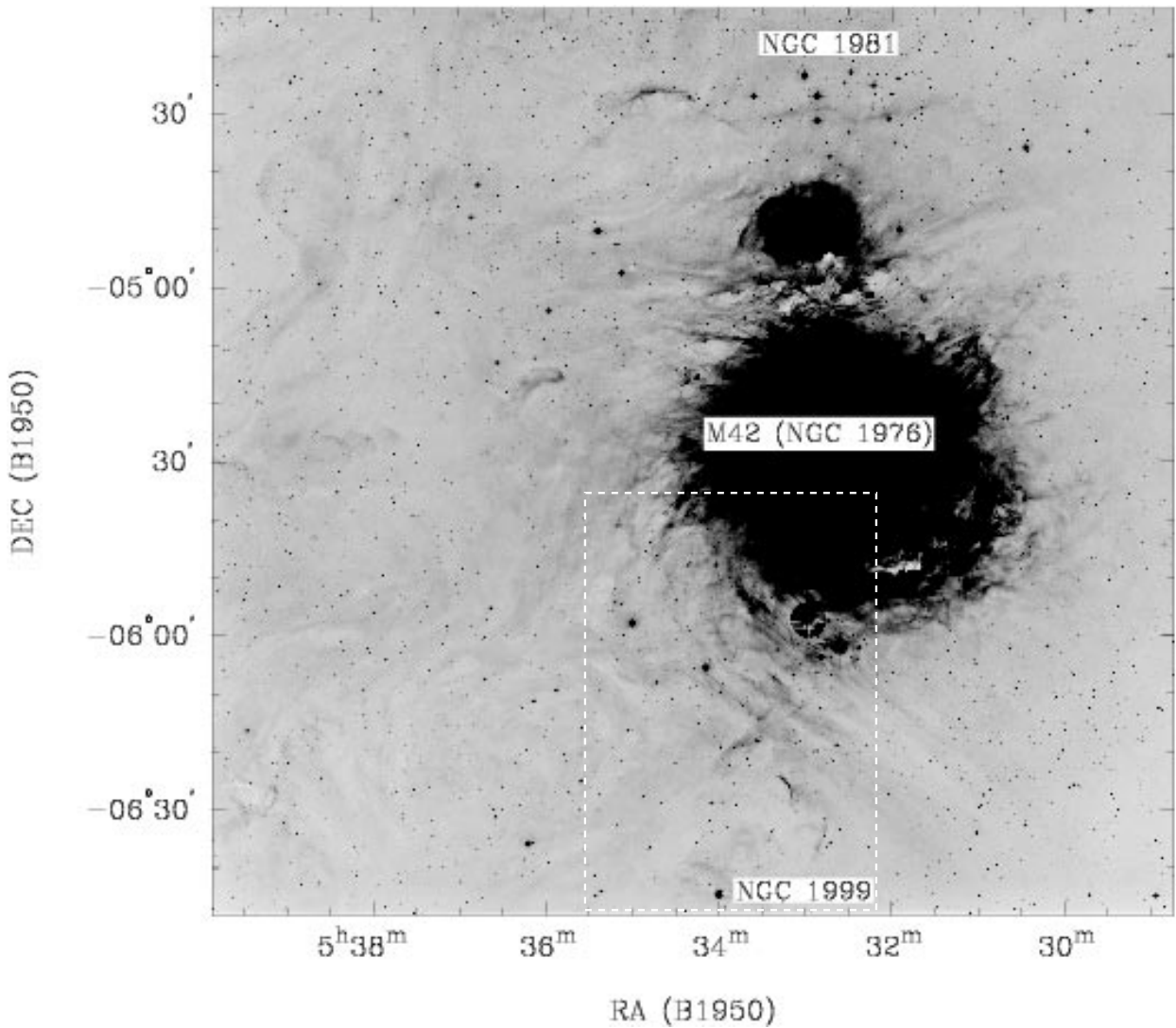


Figure 5. Unsharp-mask $H\alpha$ scan of the L1641 survey region. The northern extent of L1641 is indicated by the bright ionisation rim near the open cluster NGC 1981. The bright $H\text{II}$ region M42 (NGC 1976) is surrounded by highly structured filaments with several cometary globules seen to the east. The southern portion of the image is bounded by the reflection nebosity NGC 1999. The box outlines the region shown in Fig. 6 where a large number of HH objects have been identified.

by the bright ionization front near the open cluster NGC 1981. The cloud extends several degrees south of the figure. The $H\alpha$ emission surrounding the bright $H\text{II}$ region M42 shows remarkable substructure. The southern portion of the image is bounded by the bright reflection nebosity NGC 1999. In contrast to the L1630 region, we have identified 15 HH complexes within the outlined region shown in Fig. 5. The region is shown in more detail in Fig. 6, where the new objects and features of note are indicated. Several strings of objects appear to extend to the north and north-east of the figure. The outlined region towards the centre of Fig. 6 contains a cluster of objects surrounding the high-luminosity source IRAS 05338 – 0624 ($L_{\text{bol}} \sim 220 L_{\odot}$).

3.2.1 HH 292 (Figs 6 and 7)

Located in the south-eastern portion of Fig. 6, BE Ori (=HBC 168; IRAS 05345 – 0635) is a classical T Tauri star with $W(H\alpha) > 10 \text{ \AA}$ (Cohen & Kuhl 1979; Strom, Margulis & Strom

1989a). No molecular outflow was detected by Levreault (1988a,b). The near-infrared photometry of Strom et al. (1989a) indicates excess emission, suggesting the presence of a remnant circumstellar disc.

In Fig. 7, our scanned $H\alpha$ and CCD images clearly show a highly collimated flow originating from BE Ori. The flow has also been identified by Reipurth (private communication). On the $H\alpha$ scan (Fig. 7a), knots B–D appear to be linked by a stream of $H\alpha$ emission which could be interpreted as a jet. BE Ori itself is surrounded by diffuse $H\alpha$ emission which extends towards knot A, which is to the south-west of the source. All these features are confirmed by our $H\alpha + [\text{S II}]$ and continuum images (Figs 7b and c). All knots appear $H\alpha$ -bright with knot B displaying a combination of emission and continuum emission. Designated HH 292, the flow extends along $\text{PA} = 45^\circ$ with knot A located 114.7 arcsec to the south-west and knots B–D located 21.2, 47.3 and 64.4 arcsec to the north-east of BE Ori respectively, making the total flow length 0.4 pc. In their survey of L1641, Stanke, McCaughrean & Zinnecker (1998, hereafter SMZ98) identified

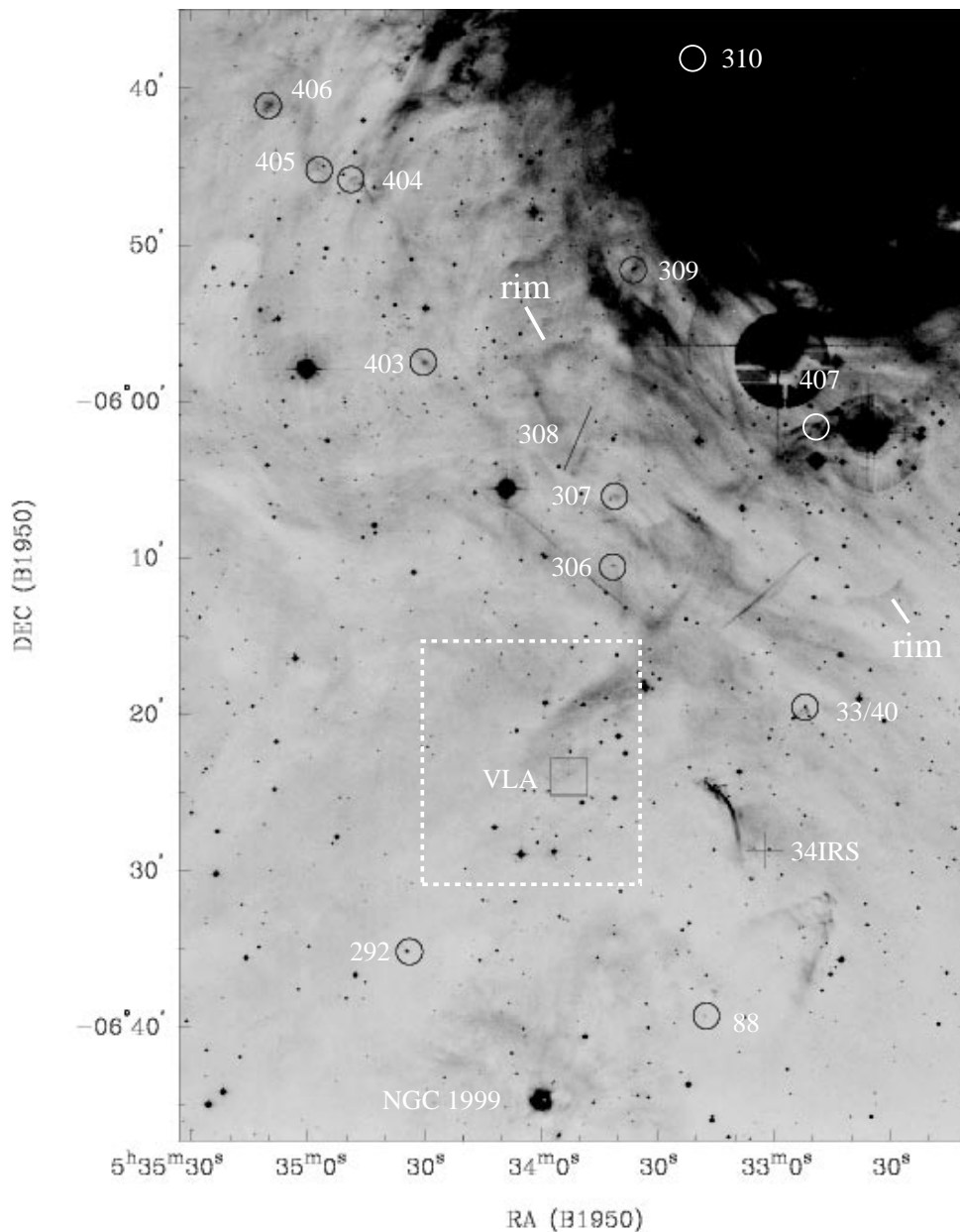


Figure 6. Scanned $H\alpha$ image of the L1641-N region outlined in Fig. 5. The $H II$ region M42 (NGC 1976) is seen to the north-west with the reflection nebulosity NGC 1999 seen to the south. New objects are numbered and indicated by a single object to avoid confusion. A large rim of $H\alpha$ emission appears to surround the HH 306–309 and 407 group. To the north of HH 309, R98 identified several bow shocks (HH 310) in the main nebulosity of M42. As a scale reference, the 3-pc flow HH 34 is shown with its northern (HH 33/40) and southern (HH 88) terminal working surfaces. The central source (34 IRS) is indicated by the cross. The bordered region (see Fig. 8) contains a cluster of objects surrounding the bright *IRAS* source *IRAS* 05338 – 0624 (marked as VLA).

compact H_2 emission associated with knots A and D (SMZ 25), which may represent the terminal working surfaces of the flow where the wind is encountering dense material.

It is interesting to note the asymmetry in HH emission with respect to BE Ori. The lack of optical counterparts to knots B–D to the south-west of the source suggests that BE Ori either has undergone highly irregular outbursts in the past, or has a one-sided jet (Rodríguez & Reipurth 1994). Assuming a tangential flow velocity of 150 km s^{-1} , knots B–D have ages of approximately 300, 700 and 1000 yr respectively, suggesting periodic outbursts every 300–400 yr, whereas knot A has an age of 1700 yr. As the seeing during our observations of BE Ori was ~ 3 arcsec, deeper

imaging may reveal further HH emission and constrain the ejection history of the source.

3.2.1.1 The L1641-N region. In Fig. 8, we present scanned $H\alpha$, IIIaF and IVN images of the outlined region in Fig. 6 where a cluster of faint red nebulosity objects was found by Reipurth (1985). The region has been mapped in ^{12}CO by Fukui et al. (1986; 1988) who found a bipolar outflow, L1641-N, centred on the bright far-infrared source *IRAS* 05338 – 0624. Near-infrared imaging of the region by Strom, Margulis & Strom (1989b), Chen et al. (1993) and Hodapp & Deane (1993) revealed a dense cluster of approximately 20 members surrounding the *IRAS* source. Davis

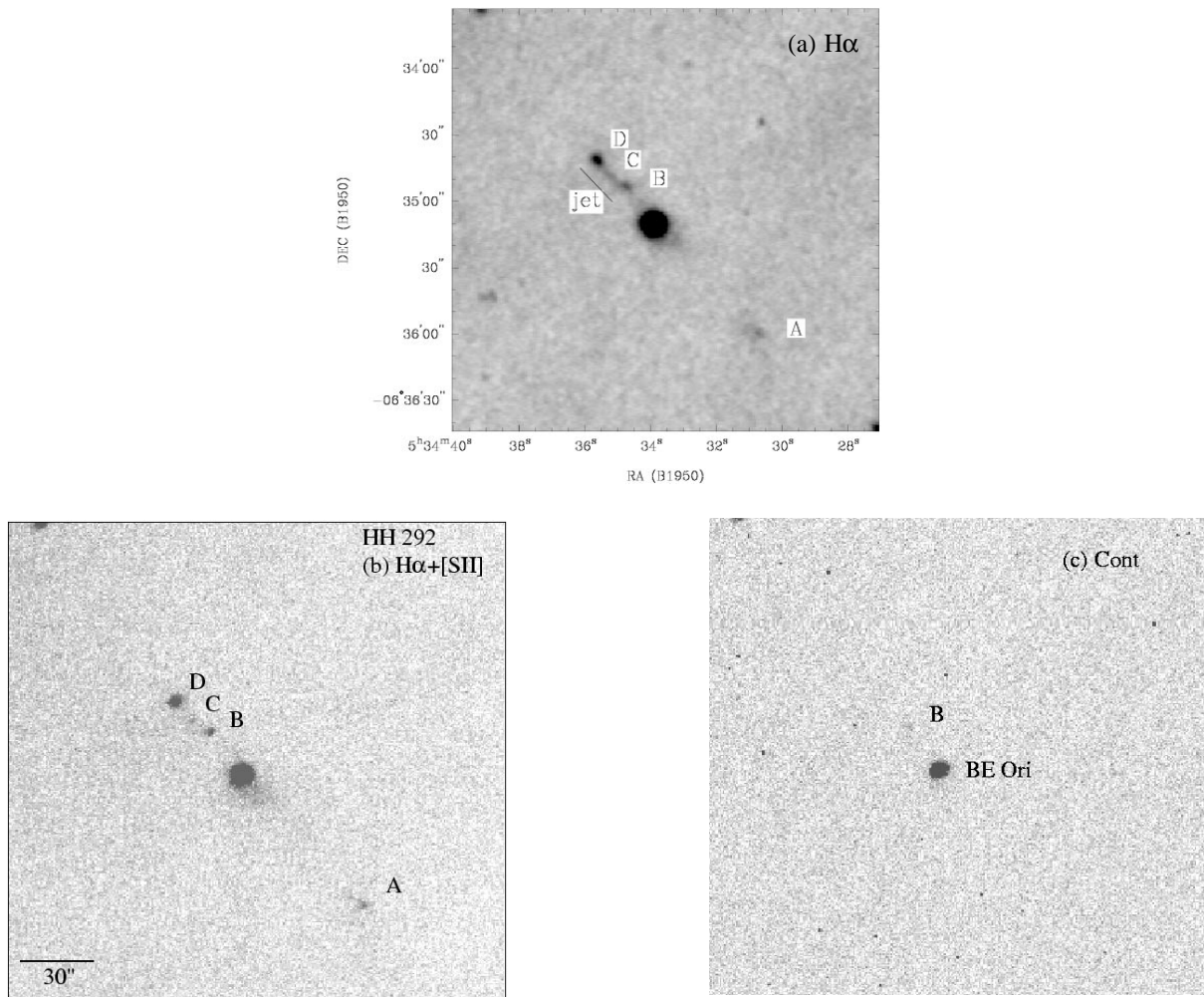


Figure 7. (a) Scanned $H\alpha$ image of BE Ori and the HH 292 outflow. A stream of $H\alpha$ emission, or jet, links three knots (B–D) to the north-east, while a further $H\alpha$ knot (A) is seen to the south-west. (b) CCD $H\alpha + [S II]$ and (c) continuum images of HH 292. HH 292B comprises both emission and continuum emission.

& Eislöffel (1995, hereafter DE95) and SMZ98 identified a multitude of H_2 ($2.12 \mu\text{m}$) emission which outlines a cavity bored out by the CO outflow, and multiple jet and bow shock features which extend at least 2 pc to the south of the embedded cluster.

In the following, we present our CCD images of the region shown in Fig. 8 which confirm many of the Reipurth nebulosities as bona fide HH objects. Scanned $H\alpha$ images for several of these objects are also presented by Parker & Phillipps (1998b). Independent CCD imaging of the region has also been presented by R98. Candidate energy sources for these flows are presented based on their location with respect to the optical and near-infrared emission (DE95; SMZ98).

3.2.2 HH 301/302 (Figs 8 and 9)

Extending to the east of the region shown in Fig. 8, the combined $H\alpha + [S II]$ image of these two objects (Fig. 9a) shows that HH 301 consists of three bright knots (A–C) which form a U-like structure with several fainter knots (D–F) trailing to the south-west. Likewise, HH 302 consists of one bright knot (A) with a fainter one (B) extending to the south-west. Both objects are brighter in $[S II]$ with faint $H\alpha$ emission. This property is apparent from Figs 8(a) and (b),

where HH 301/302 are prominent on the IIIaF, but faint in the $H\alpha$ image. R98 suggest that HH 301/302 are related, based on their elongation towards the L1641-N embedded cluster where the presumed driving source is located. A line of $[S II]$ emission can be seen to the south which mirrors the position of HH 301/302 and coincides with H_2 emission (SMZ 17/18). The bright knot HH 298A (R98) can also be seen in Fig. 9(a). Although R98 list HH 298 as being 70 arcsec in extent with an east–west orientation, our $H\alpha + [S II]$ image shows that HH 298 extends even further to the east of HH 298A with several knots which we label as HH 298D–F. This makes the HH 298 flow 340 arcsec or 0.76 pc in length from knots A to F. It is interesting that, together with HH 301/302, HH 298 produces a V-type structure with the apex pointing back towards the infrared cluster.

DE95 and SMZ98 identified a chain of H_2 knots (I/J and SMZ 16A/B respectively) which extend east from the embedded cluster with a morphology reminiscent of a jet. In fact, HH 298A appears directly between SMZ 16A and B. As HH 298 and 301/302 contain both optical and near-infrared emission, we suggest that they are tracing the walls of a cavity outlined by the V-type structure. The presence of a jet (SMZ 16A) and counterflow (HH 298A and SMZ 16B) suggests that we are seeing a single outflow

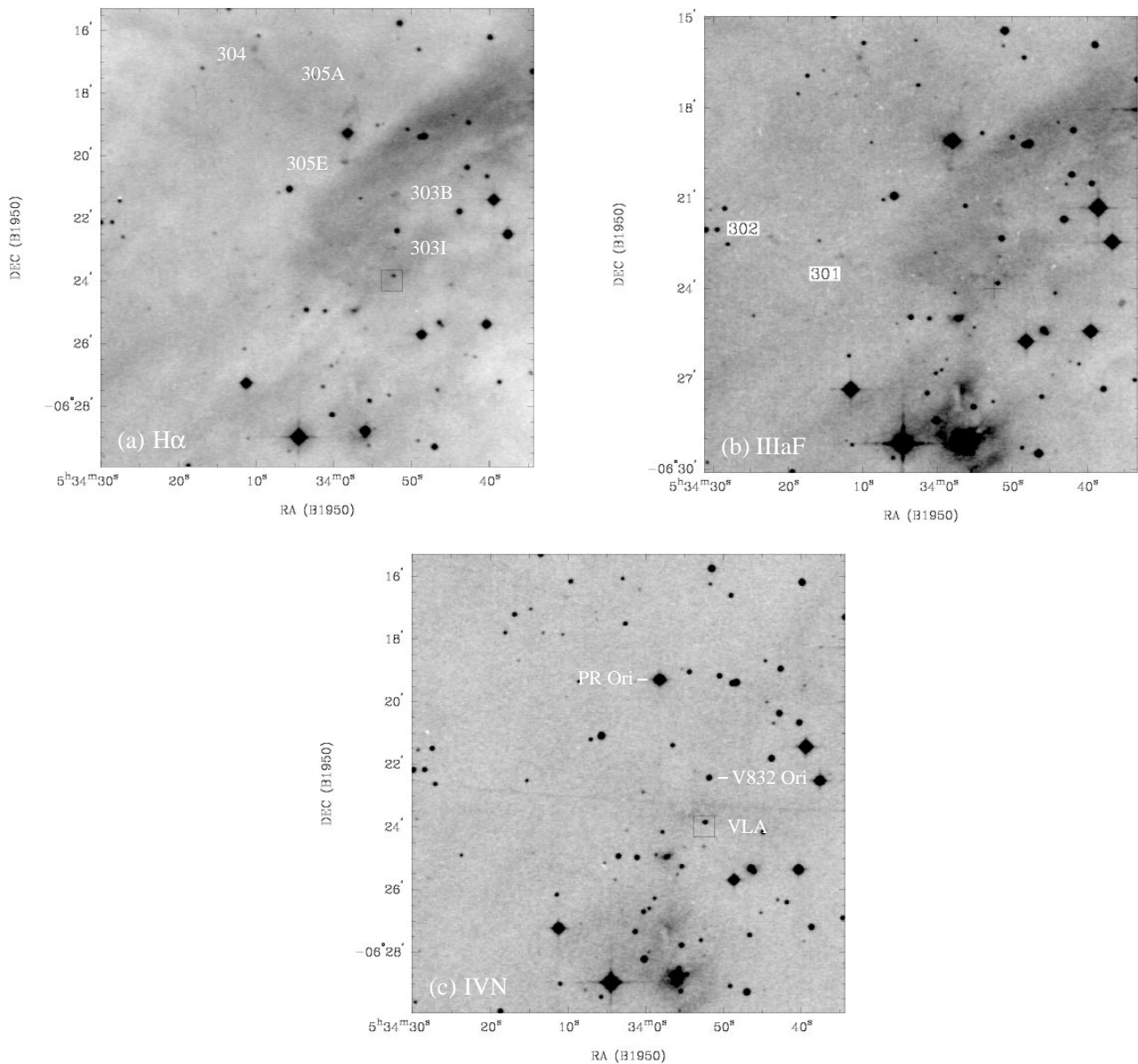


Figure 8. Scanned (a) $H\alpha$, (b) IIIaF and (c) IVN images of the region outlined in Fig. 6. Note that many of the nebulosities on the IIIaF are rather faint in comparison with their appearance in $H\alpha$. The indicated nebulosities are absent from the IVN image, confirming that they are pure emission-line objects. The emission-line stars PR Ori and V832 Ori are indicated, with the location of the VLA outflow source indicated by the box in all images.

complex. As the jet extends directly between HH 298 and 301/302, we do not rule out the possibility of three separate flows, although we draw a comparison with the outflow source L1551-IRS5, where HH 28/29 are not located along the jet axis, but are close to the walls of a cavity identified by optical, near-infrared and CO observations (see Davis et al. 1995, and references therein).

Chen et al. (1993) identified a K' -band source (their N23) in the direction of DE95 I/SMZ 16B which is not visible in our I -band image (Fig. 9b). Based on the alignment of optical and near-infrared emission, we propose this source as the driving agent for both HH 298 and 301/302. Further spectroscopic studies are needed to clarify its nature.

3.2.3 HH 303 (Figs 8 and 10)

The HH 303 flow consists of two groupings of knots aligned along

a north–south direction. The $H\alpha + [S II]$ image in Fig. 10(a) shows that the northernmost group (knots A–F) outlines a bow shock with a sheath of $H\alpha$ emission overlying clumpy $[S II]$ emission. Several more $[S II]$ -bright knots (I–K) extend towards the south. A fainter knot, HH 298A (R98), is seen to the south-west of knot K. However, fig. 5 of R98 shows HH 298A at a different location from that shown in Fig. 10(a). Therefore, we identify this knot as HH 303L in continuation of R98. R98 suggests that HH 303L may be associated with HH 303, but deviates too much from the well-defined axis and may represent a separate flow. We suggest that knots I–K and L represent a remnant bow shock with the former and latter representing the eastern and western wings respectively.

At first glance, HH 303 could be interpreted as a highly collimated flow originating from the variable star V832 Ori (Fig. 10b). The optical and near-infrared photometry of this source (source N2 of Chen et al. 1993) shows a spectral energy

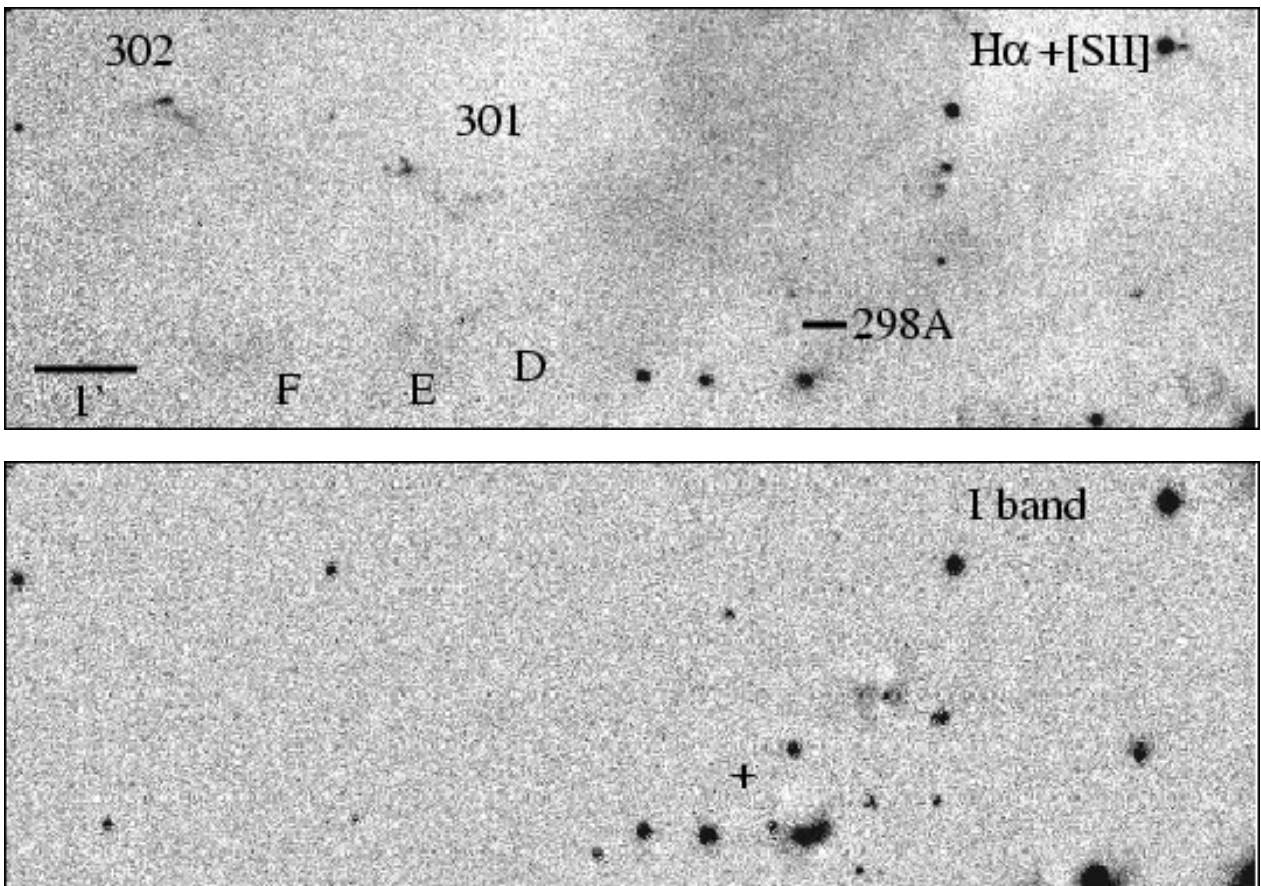


Figure 9. (a) $H\alpha + [S II]$ and (b) I -band images of the HH 298, 301 and 302 outflows identified from Fig. 8. The cross in the I -band image marks the location of the presumed energy source (N23 of Chen et al. 1993) for HH 298/301/302.

distribution which declines rapidly for $\lambda > 1 \mu\text{m}$, suggesting a lack of circumstellar material. A comparison of our optical images with the near-infrared data of SMZ98 shows that most of HH 303 displays both optical and H_2 emission, thereby suggesting that HH 303 is behind V832 Ori and unrelated to the star. Knots HH 303B, F and I are coincident with the H_2 knots SMZ 8A, 8B and 14P respectively, with the H_2 emission displaying bow shock morphologies which open towards the south in the direction of L1641-N.

As knots HH 303I–K lie within the blue lobe of L1641-N, it has been suggested the CO, near-infrared and optical flows derive from a common source (Strom et al. 1989b; SMZ98; R98). Chen et al. (1993) identified a bright M -band source (their N15) ~ 8 arcsec to the east of the *IRAS* position. Chen, Zhao & Ohashi (1995) detected this source with the VLA at 2.0 mm, 7.0 mm and 1.3 cm, while SMZ98 identified a 10- μm source coincident with N15 and the VLA source. As N15, the 10- μm source and the 1.3 cm source represent the same object, we follow R98 and label it as the ‘VLA source’ which they suggest is the driving source for HH 303 and the illuminator of the reflection nebulosity seen to the north-east in our I -band image (HD 93; Fig. 10b).

However, it is important to mention that the L1641-N region is a highly clustered environment where identifying outflow sources requires the highest resolution possible. Anglada et al. (1998) identified two radio continuum sources, VLA2 and VLA3, which are 0.8 and 0.2 arcsec to the west and east respectively from the nominal position of the VLA source. Further observations of the

region reveal a fainter source within 1 arcsec of VLA2 (Anglada, private communication). The CO data of Fukui et al. (1986, 1988) clearly indicate that the L1641-N molecular outflow is more complex than a simple bipolar outflow. Higher resolution studies of these sources are needed to determine which source is driving the optical and H_2 emission. In particular, it would be interesting to see if the VLA source displays an elongated radio jet with its long axis pointing in the direction of HH 303.

In addition to HH 303, R98 suggest that the VLA source also drives HH 61/62, which are located 46.8 arcmin (6.5 pc) to the south of L1641 (see Fig. 18, later). If their assumption is correct, the HH 61/62/303 flow is 7 pc in length, with the northern lobe only 5 per cent the length of the southern lobe. Any shocks associated with the northern lobe will be extremely faint owing to the lack of molecular material as the flow moves away from L1641.

3.2.4 HH 304 (Figs 8 and 11)

Located to north-east of the VLA source, the $[S II]$ image of HH 304 (Fig. 11a) shows several compact knots which are $[S II]$ -bright. Knot B is compact with a bow shock structure (knot A) extending towards the north-east and then curling back to the north-west. Knots C and D display an opposing bow shock structure, with knots C and D connected by faint $[S II]$ emission. The overall morphology of the system suggests that the energy

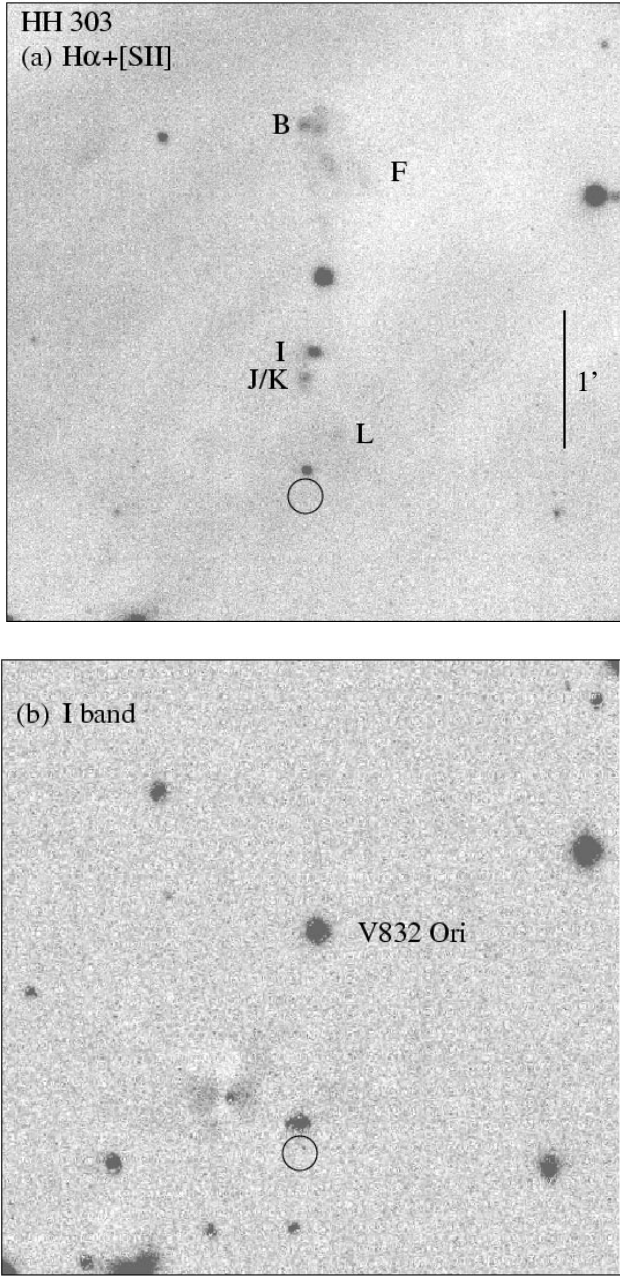


Figure 10. (a) $H\alpha + [S II]$ and (b) I -band images of the HH 303 complex identified from Fig. 8. The circle marks the location of the VLA source, which R98 propose as the driving source for HH 303.

source is located between knots A/B and C/D. The I -band image (Fig. 11b) shows a compact reflection nebulosity with a tail which mimics part of the $[S II]$ emission associated with knots A and B. A reddened source (which we denote as HH 304IRS) appears where the reflection emission is most compact.

The HH 304 complex is also seen in the H_2 mosaic of SMZ98, who label it SMZ 5. HH 304A is seen as a bright bar which extends 6 arcsec along an east–west direction. At the position of the compact reflection nebulosity, a bright H_2 knot is seen, with a trail of H_2 emission extending from HH 304IRS towards HH 304C. The appearance of the optical and near-infrared emission suggests that we are seeing two lobes with knots A and C representing the north-eastern and south-western working surfaces

respectively. HH 304IRS appears mid-way between these two opposing working surfaces. There are no *IRAS* or $H\alpha$ emission-line stars at the location of the reflection nebulosity, which implies a deeply embedded source.

3.2.5 HH 305 (Figs 8 and 12)

The HH 305 outflow appears aligned along a north–south axis centred on the bright ($V \sim 11.3$ mag) star PR Ori. With the exception of knots A and F, all objects are $H\alpha$ -bright, with knot B displaying an inverted V-type structure only visible in $H\alpha$. Knot A shows a bow shock structure which opens towards PR Ori. It is interesting to note that HH 305E represents the brightest nebulosity in the flow. The increased brightness could be attributed to the flow encountering an obstacle of some sort, perhaps in the form of a molecular clump. The dark lane seen in Figs 6, 8 and 12 represents a change in the molecular distribution in this part of L1641. At the position of HH 305E, the flow impacts the molecular cloud and then deflects to where we see HH 305F. Based on their separation from PR Ori, R98 suggest that knots C/D represent an HH pair located 16 arcsec from the source. Similarly, knots B/E and A/F represent HH pairs located 65 and 108 arcsec from PR Ori respectively, making the total flow length 0.54 pc.

At present, it is unknown if HH 305 is being driven by PR Ori or a more embedded source behind it (R98). In a major study of *Einstein* X-ray sources in L1641, Strom et al. (1990) identified PR Ori as a low-luminosity ($13 L_{\odot}$) source with a spectral type of K4e α and $W(H\alpha) = 0.5 \text{ \AA}$. Their *JHKLM* photometry indicates a lack of infrared colour excess normally attributed to a circumstellar disc. Based on their data, PR Ori appears to be a weak-lined T Tauri star (wTTs). Its location with respect to the L1641 molecular cloud shows that it lies in a region of low obscuration and, in addition to the fact that SMZ98 did not detect any H_2 emission associated with HH 305, is not consistent with the notion of an embedded, younger source located behind PR Ori.

If PR Ori were the energy source of HH 305, it would present a major discrepancy in star formation theory, as wTTs are not thought to be associated with circumstellar discs and/or outflow phenomena. Magazzu & Martin (1994) identified what was thought to be an HH flow associated with the wTTs HV Tau. Woitas & Leinert (1998) suggested that the HH object is actually a companion T Tauri star with strong forbidden emission lines, the presence of which originally led Magazzu & Martin to their conclusions. How do we reconcile the fact that PR Ori is a wTTs with an outflow? The answer may lie in table 2 of Strom et al. (1990), who list PR Ori as an optical double. Our CCD images also show PR Ori as an extended source, in which case it seems more plausible that the companion (PR Ori-B) is the driving source of HH 305. Clearly, further studies of this HH complex are needed.

3.2.6 HH 306–309 (Figs 6 and 13–16)

Figs 6 and 13 show scanned $H\alpha$ and IVN images of a string of emission-line objects (HH 306–309) extending away from the VLA source and up into the main reflection nebulosity of M42. A large arcuate structure (HH 407) can be seen near the bright stars towards the western border. The large rim of $H\alpha$ emission identified in Fig. 6 is seen orientated at $PA = 55^\circ$ and appears to

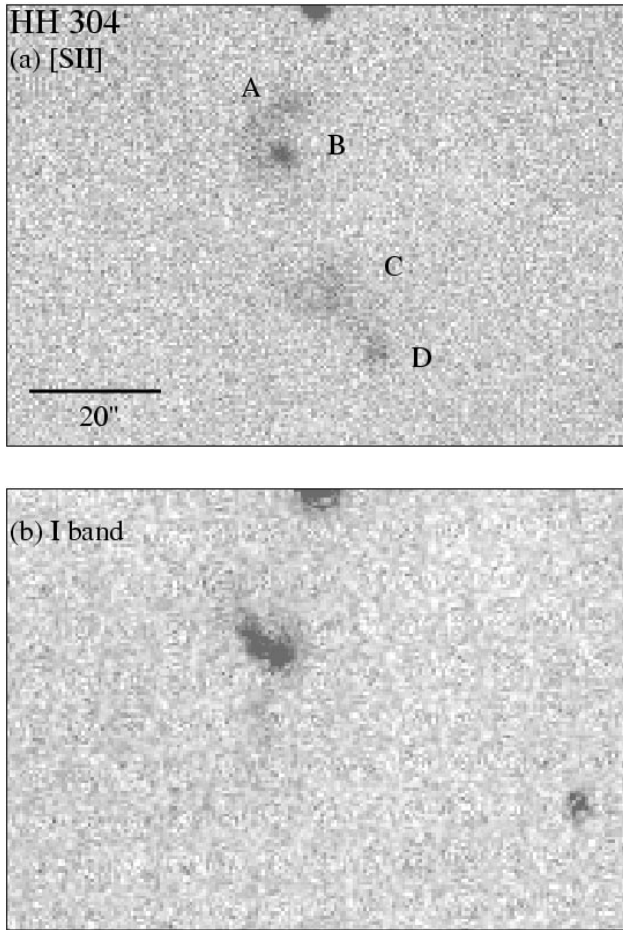


Figure 11. (a) [S II] and (b) *I*-band images of the HH 304 outflow located in the north-east of Fig. 8. Knots A/B and C/D represent opposing bow shocks with a reddened source located at knot B. The candidate energy source (HH 304IRS) displays a fan of reflection nebulosity extending to the north-east.

surround all objects in the figure. A comparison of the $H\alpha$ and IVN images confirms that all objects are pure emission-line features.

3.2.6.1 The HH flows. In conjunction with the IVN image (Fig. 13b), our $H\alpha + [S II]$ images confirm all as bona fide HH objects. In Fig. 14, the $H\alpha + [S II]$ image shows that HH 306 consists of two bright compact knots (B and F) with a trail of emission extending to the south. A further knot, HH 306G, lies to the west and may be unrelated, or part of an older fragmented shock. HH 307 consists of several bright knots which mark the apexes of large arcs or wings which sweep out and open towards L1641-N. R98 suggest that HH 308 appears as a fragmented bow shock with knots A and B representing the eastern and western wings respectively. Located between HH 308A and B, we note the presence of a third knot not identified by R98 which we denote here as HH 308C. HH 309 (Fig. 15) shows a similar structure to HH 308, with knots A and B representing the first fragmented bow shock, knot C the second and knots D/E the third. The reverse bow shock morphology of HH 309B can be explained by noting the distribution of $H\alpha$ emission on the scanned $H\alpha$ and CCD $H\alpha + [S II]$ images. The knot appears to have curled around the

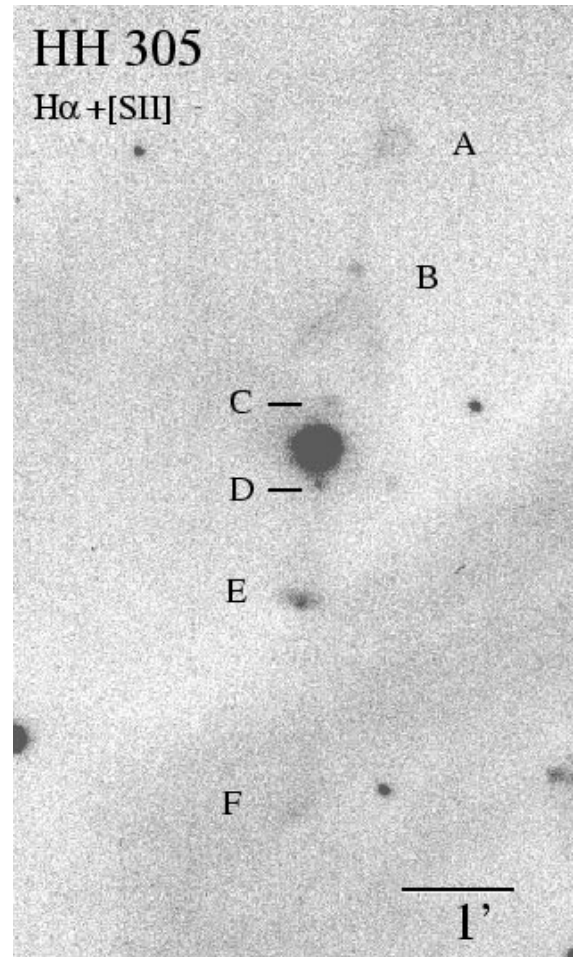


Figure 12. $H\alpha + [S II]$ image of the HH 305 flow identified from Fig. 8. Knot E marks the location where the flow may be deflected by a dense region indicated by the darkened strip seen to the south of the image. Note that PR Ori appears slightly extended and is in fact an optical double, where the companion is the proposed energy source for HH 305 (see text).

background emission which may have been responsible for creating the fragmented appearance of HH 309.

In searching for further emission north of HH 309, R98 discovered several bow shock structures, designated HH 310, within the main nebulosity of M42 (see Fig. 6). The objects are brighter in [S II] than in $H\alpha$, thus discounting the possibility that they might be photoionized rims. We have also imaged these structures and, for completeness, present our $H\alpha$, [S II] and continuum images in Fig. 16. Our [O III] frame (not shown) does not detect the bow shocks associated with HH 310, thereby suggesting that the flow is moving with a velocity less than 100 km s^{-1} . Our [S II] and continuum images (Figs 16a and b) identify several bow shock structures to the north-west of HH 310 which are [S II]-bright and absent in the continuum frame. Assuming for the moment that these features are bona fide HH objects, their apparent deviation from the axis defined by HH 310 can be explained if the flow is being redirected by an obstacle, possibly the long tongue-like feature which extends from the top of the images. An alternative explanation is that they form part of a separate flow, perhaps from the L1641-N region. Spectroscopic observations of these features are needed to determine if they are HH shocks.

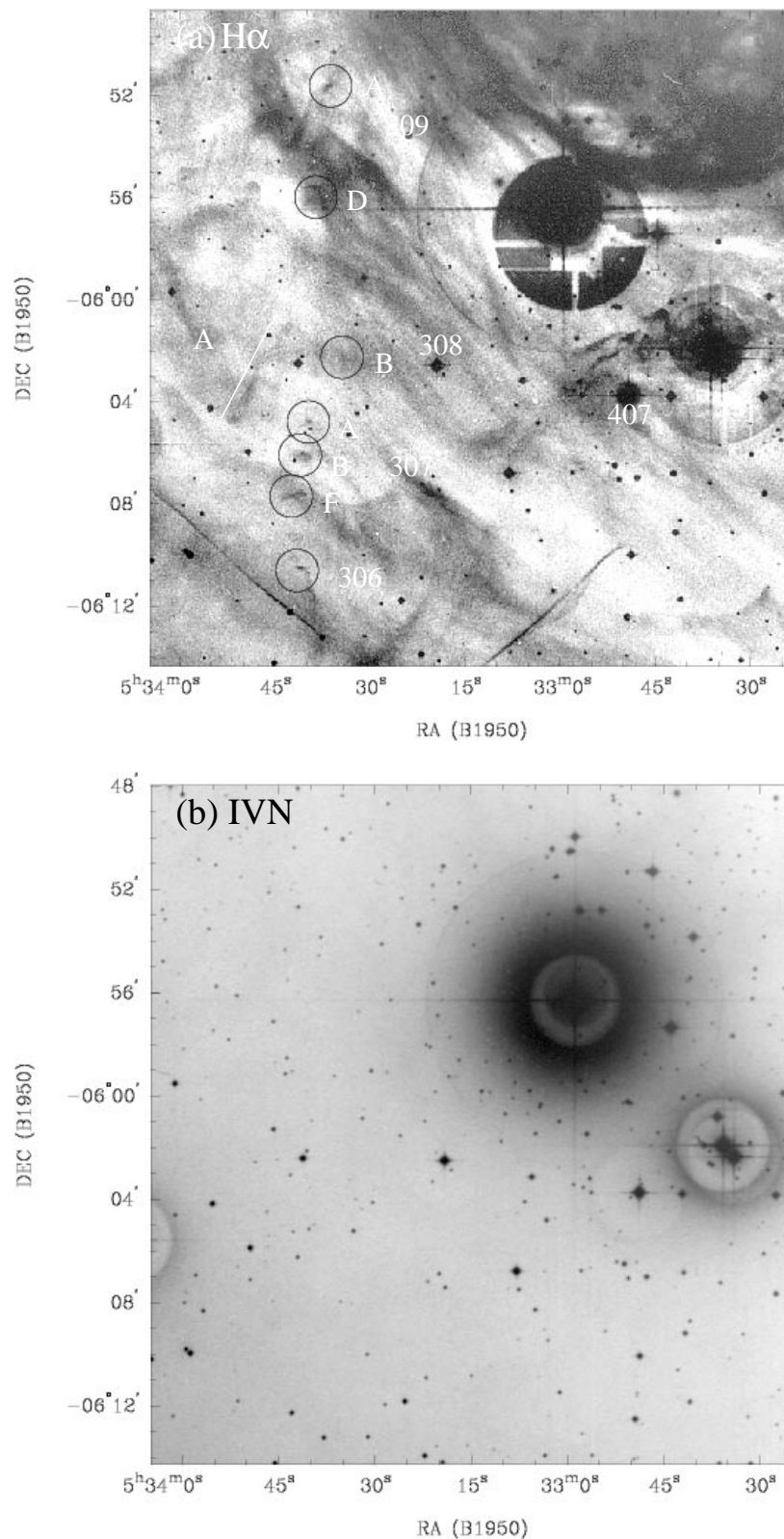


Figure 13. Scanned (a) $H\alpha$ and (b) IVN images of the northern objects HH 306–309 and 407 identified in Fig. 6. The large rim of $H\alpha$ emission is clearly visible and, as no emission is seen in the IVN image, the rim is identified as a pure emission-line feature.

3.2.6.2 *The embedded counterflow.* To the south of L1641-N, SMZ98 discovered a long chain of bow shocks. Designated SMZ 23, the chain consists of at least seven bow shocks (A–G) which may represent the redshifted counterflow to HH 306–310 (R98;

this paper). From the ^{13}CO data of Bally et al. (1987), the integrated moment map (Fig. 17) shows evidence of a cavity created by SMZ 23. What are interesting about this cavity are its size and orientation with respect to L1641-N, HH 306–310 and

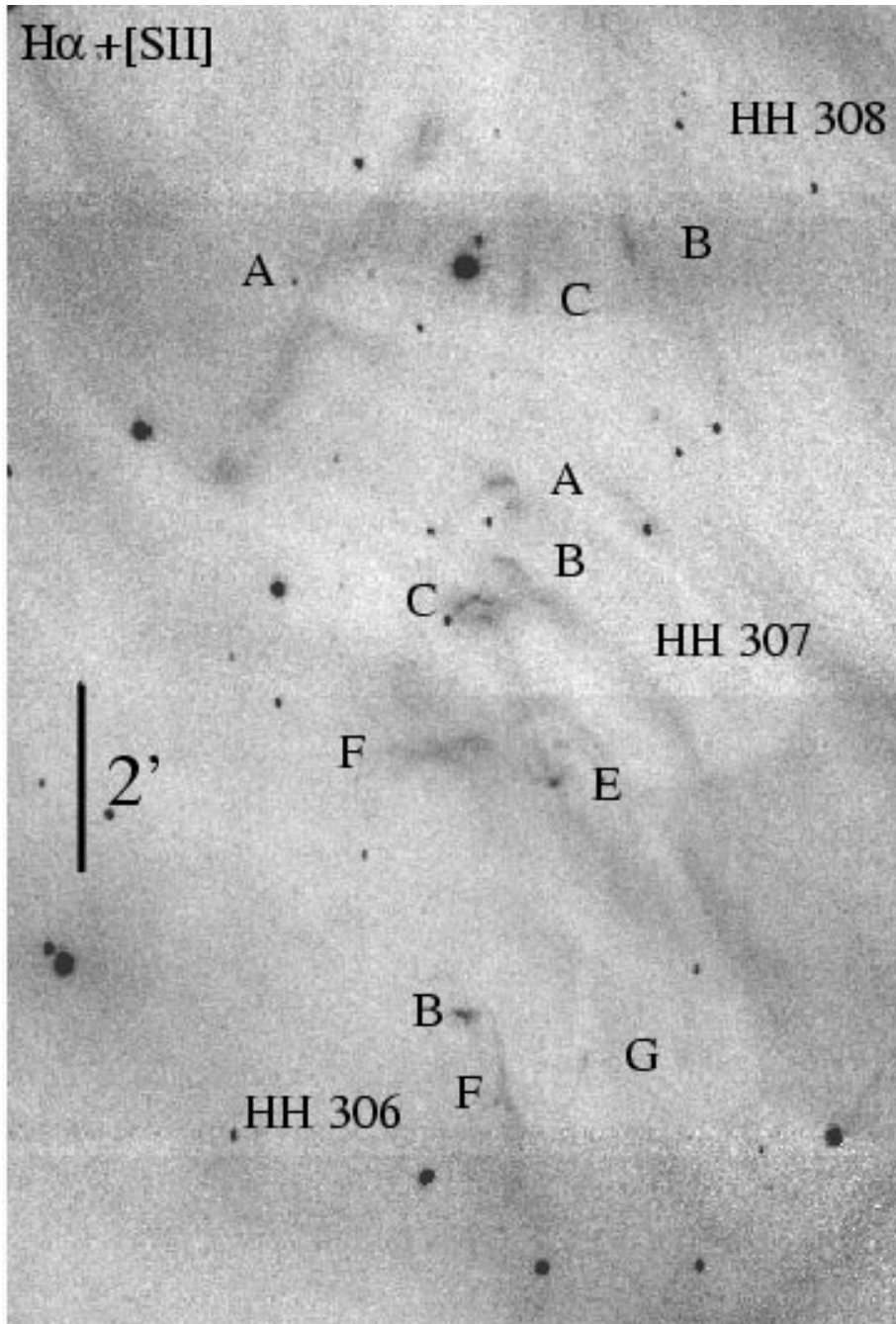


Figure 14. $H\alpha + [SII]$ image of HH 306–308. In addition to several bright knots, the HH 307 bow shock clearly displays larger bow shock structures which open to the south and have the bright knots at the apexes of the bows. HH 308 appears as a highly fragmented bow shock, with HH 308A displaying an elongated structure (see text for details).

the large cavity dubbed by R98 as the ‘L1641-N chimney’, which they suggest has been excavated by the repeated passage of bow shocks associated with HH 306–310. The locations of individual knots associated with SMZ 23 appear to trace the western wall of the southern cavity, suggesting that the flow impacts with the cavity wall which produces the observed emission. We suggest that this southern cavity is being excavated by SMZ 23 as the redshifted flow propagates into and away from L1641-N. The ^{13}CO velocity structure of the southern cavity is evident from 5 to 8 km s^{-1} , with the L1641-N molecular core and the ‘L1641-N chimney’ appearing around 8 and $8\text{--}11 \text{ km s}^{-1}$ respectively. This

gives further evidence that the southern cavity and the ‘L1641-N chimney’ represent expanding red- and blueshifted lobes centred on the L1641-N region.

Following similar arguments in R98, we find the dimensions of this southern cavity to be $5 \times 12 \text{ arcmin}^2$, giving a total area of $\sim 1 \times 10^{37} \text{ cm}^2$. Assuming that the intensity in the cavity lies within $3\text{--}5 \text{ K km s}^{-1}$, the total mass excavated by the SMZ 23 flow is $\sim 37\text{--}62 M_{\odot}$. In comparison, R98 find that HH 306–310 have removed $\sim 190 M_{\odot}$ of gas from L1641. Apart from obvious errors in estimating the ^{13}CO intensity and cavity size, we should point out that we have not taken into account the possibility that

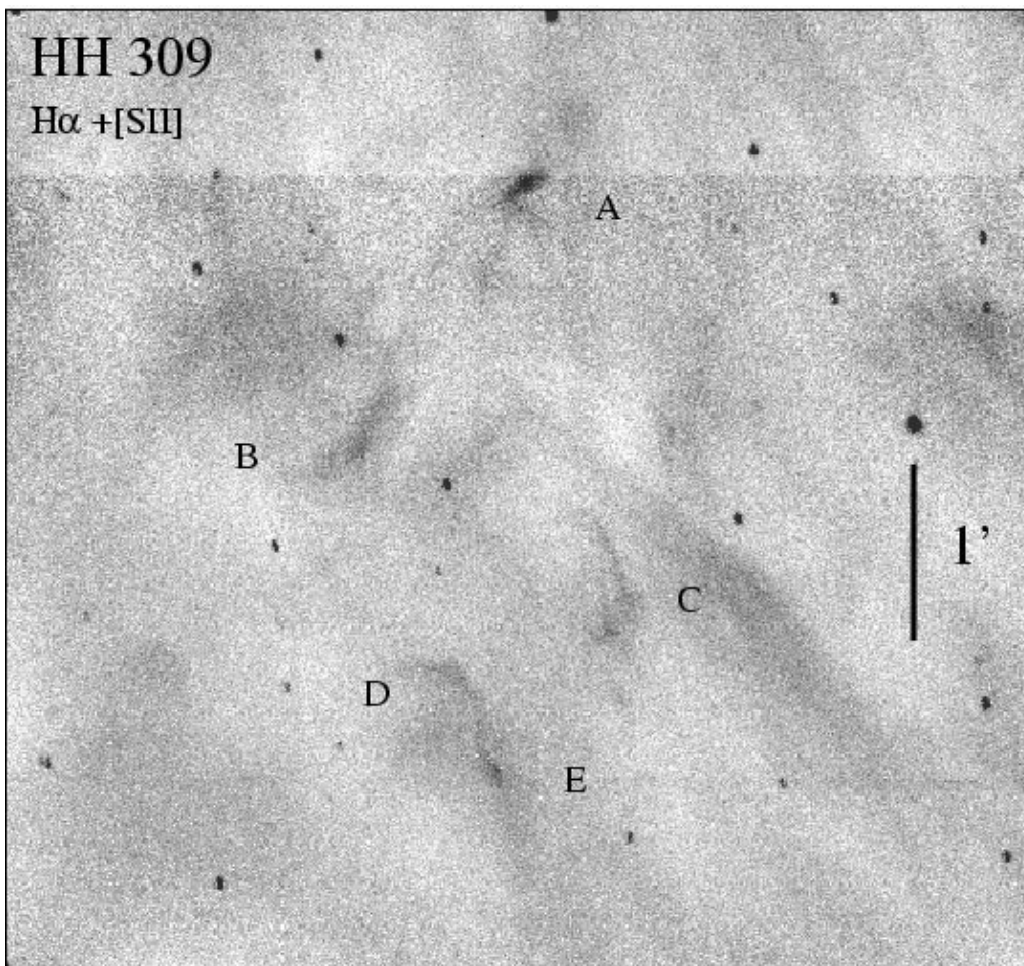


Figure 15. $H\alpha + [S II]$ image of the HH 309 bow shock. The reverse morphology of knot B can be explained as the flow passes over the background $H\alpha$ emission which extends from the north-east to the south-west of the figure.

the southern cavity may have been formed by the combined action of more than one outflow.

SMZ 23, HH 306–309 and HH 310 all display large bow shock structures which open towards the L1641-N region where the presumed energy source lies. As mentioned for HH 303, the high degree of clustering about the VLA source confuses identification of specific energy source(s). However, the principal components HH 306B, 307A, 308C and 309A are located 806, 1152, 1331 and 1955 arcsec away from the position of the VLA source. In addition to HH 310A (2764 arcsec), the HH 306–310 lobe is 6.3 pc in length. As the SMZ 23 flow appears to extend further south from SMZ 23G (Stanke, private communication), the geometry of HH 306–310 and SMZ 23 about the VLA source and VLA2/VLA3 strongly favours at least one of them as the energy source of the optical and near-infrared emission. Whichever of these sources is responsible for the observed emission, the combined length of the HH 306–310 and SMZ 23 lobes is 10.5 pc. High-resolution radio studies will be beneficial for identifying radio jets and their orientation with respect to the optical and near-infrared emission.

3.2.6.3 The southern L1641 region. In a search for optical counterparts to HH 306–310, our deep IIIaF plate of the southern region of L1641 identifies several features reminiscent of large bow shocks. The IIIaF image of these features is shown in Fig. 18, where object A appears as a diffuse feature and object B appears

as a bright nebulosity with a long curve which extends 16 arcmin to the north near object A. At first glance, object B and HH 61/62 (the counterlobe to HH 303: R98) appear to outline the eastern and western wings of a large fragmented bow shock structure. Objects C and D appear as large arc-like structures which open to the north and are 3–4 arcmin in extent. As C and D are located well away from the main cloud, our line of sight increases which may suggest that they are not physically associated with L1641. We should also note that many of the terminal bow shocks associated with parsec-scale HH flows show substantial substructure which is lacking from the IIIaF image. In order to resolve the nature of features C and D, we obtained $H\alpha$ and $[S II]$ images, but owing to variable cloud cover we were not able to classify these objects as bona fide HH objects. Deeper images and/or spectra of objects A–D are required to determine if they are photoionized regions or HH objects.

3.2.7 HH 403–406 (Figs 6 and 19)

To the north-east of Fig. 6, a second string of objects extends away from the L1641-N cluster. HH 403 and 404 are located well clear of the eastern edge of the L1641 molecular cloud. Although seeing at the time of observing was > 3 arcsec, our $H\alpha$ and $[S II]$ CCD images (not shown) did allow us to classify these features as

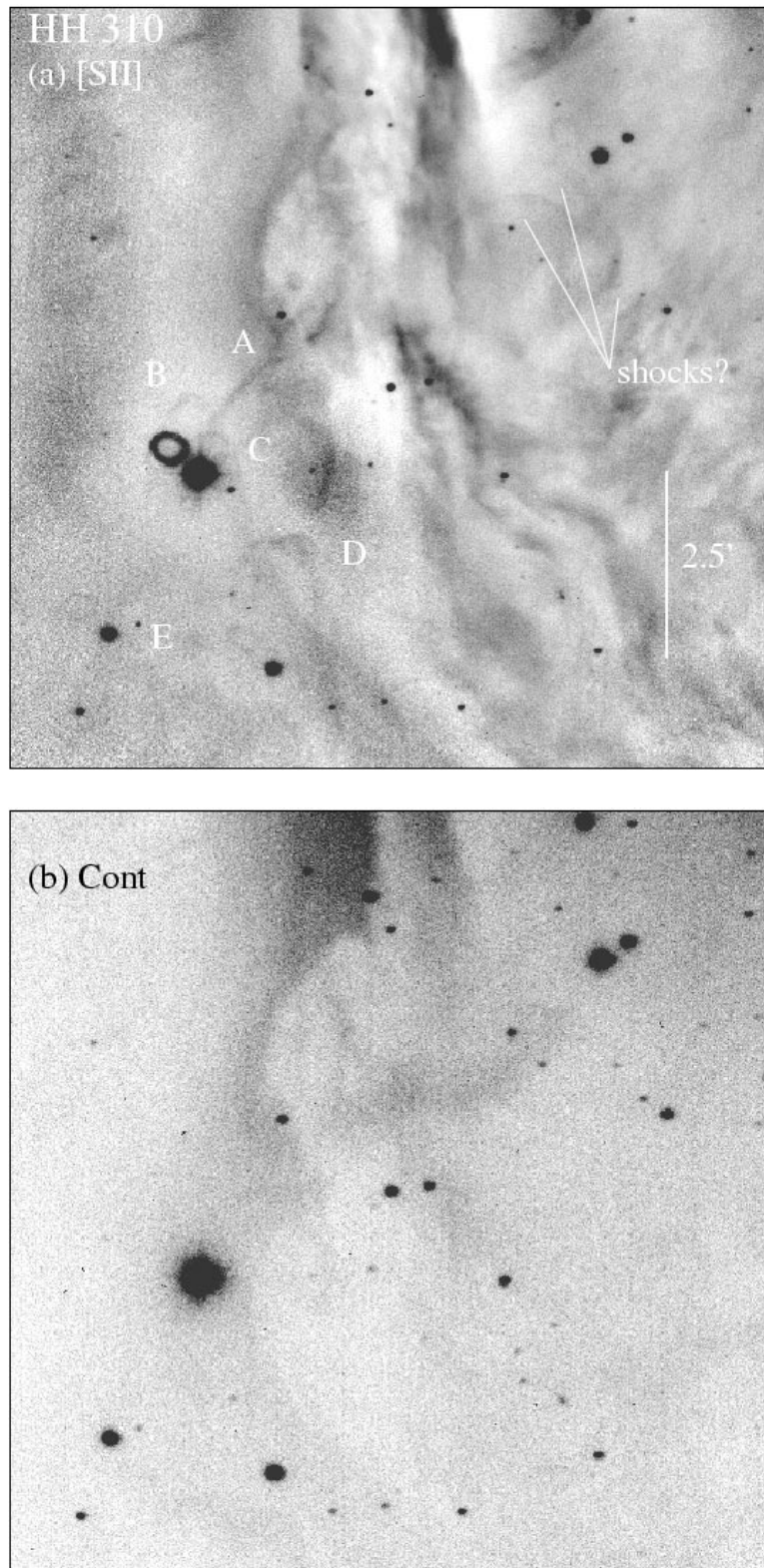


Figure 16. (a) [S II] and (b) continuum images of the HH 310 region (see Fig. 6 for location). To the north-west we see several ‘bow shocks’ which may be genuine HH objects associated with HH 310. They may be deflected from the flow axis by the tongue-like feature which extends from the top of the figure.

genuine HH objects. In Fig. 19, the scanned $H\alpha$ and IVN images show that HH 403 consists of a large number of emission-line knots in addition to curved (HH 403G) and amorphous (HH 403H) features to the south-west. The CCD images of R98 clearly show

HH 403 as a highly fragmented object which is very similar in appearance to HH 262 (López et al. 1998). A further 9 arcmin to the north-east, HH 404 displays a sickle-like structure not too dissimilar from the HH 47 jet (Heathcote et al. 1996). As these

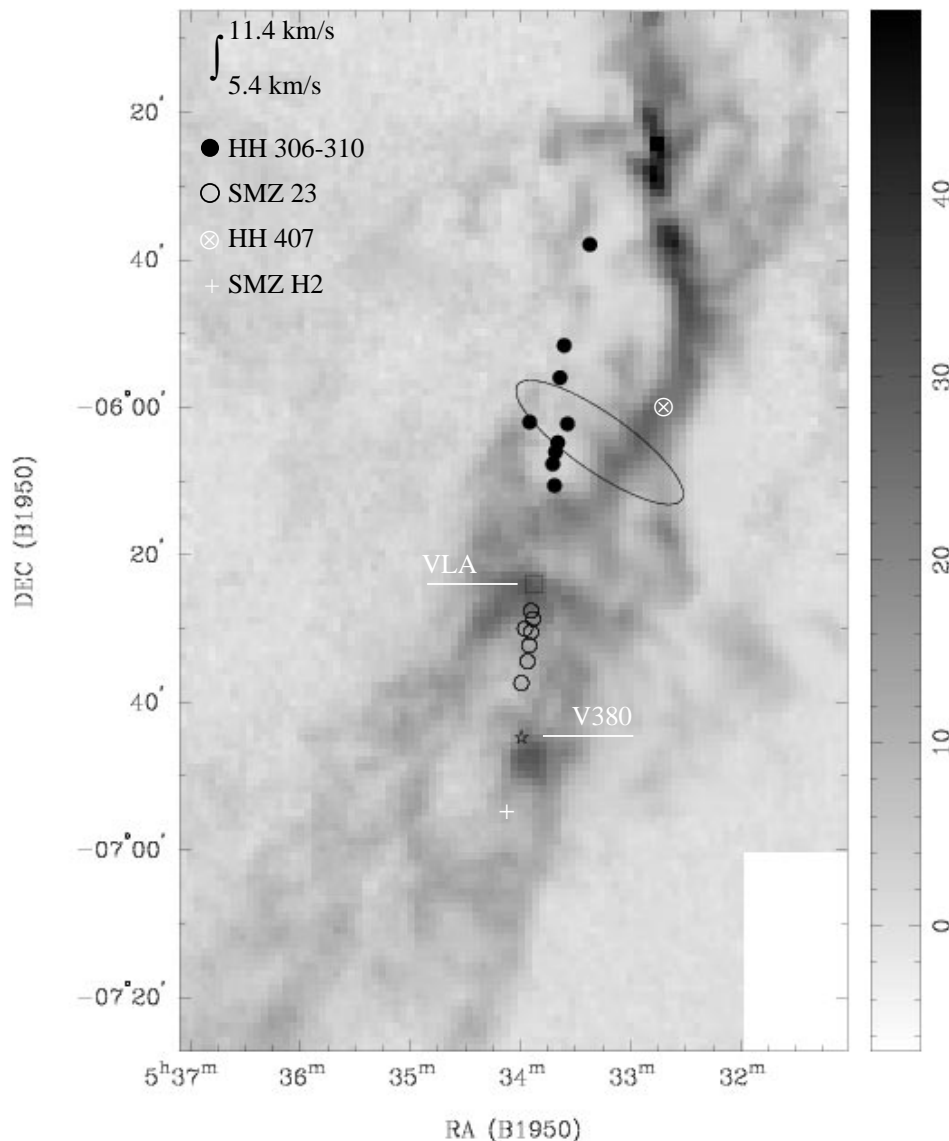


Figure 17. Integrated ^{13}CO map of the L1641 cloud from Bally et al. (1987). The emission has been integrated from 5.4 to 11.4 km s^{-1} with respect to the L1641-N cloud velocity (8.4 km s^{-1}). Filled and open circles represent the HH 306–310 and SMZ 23 flows respectively. The western wall of the southern cavity is traced by the SMZ 23 flow. A H_2 feature (+) may represent the embedded counterflow to HH 407 (\otimes). The VLA and V380 Ori outflow sources are indicated. The location of the $\text{H}\alpha$ rim with respect to HH 306–310 and 407 is indicated by the ellipse. The \int -shaped filament (Bally et al. 1987) is seen to the north and approximates the western wall of the ‘L1641-N chimney’. The wedge shows intensity in units of K km s^{-1} .

features are $\text{H}\alpha$ -bright, R98 raised the question as to whether or not HH 403/404 are bow shocks or bright rims. However, on morphological grounds, they suggest that HH 403/404 are highly fragmented bow shock structures which point back towards L1641-N where the presumed energy source lies. Our contrast-enhanced scanned $\text{H}\alpha$ image of the region (Fig. 19a) appears to confirm their suspicion, as we see a lack of background $\text{H}\alpha$ emission in the direction of HH 403/404; it has probably been removed by the action of the flow as it propagates away from L1641.

The scanned $\text{H}\alpha$ image identifies several large-scale bow shocks with HH 403 and 404 at their apexes. R98 do not detect these features on their CCD images. Originally thought to be bright rims, comparison of the $\text{H}\alpha$ emission with the ^{13}CO data of Bally et al. (1987) indicates that these ‘rims’ do not outline the L1641 molecular cloud, or any other well-defined ^{13}CO ridge. The

first bow shock is defined by the arc-like object HH 403G and HH 404H representing the eastern and western wings respectively. The eastern wing trails 7 arcmin to the south before it blends into the background $\text{H}\alpha$ emission. The second bow shock appears as an extended feature similar in appearance to HH 403G. The third bow shock only displays the western wing which extends northward from the second bow to the apex of HH 404; this shows a bright arc and faint $\text{H}\alpha$ emission which combine to form an inverted U-type structure.

North-east of HH 404, the faint object HH 405 displays $\text{H}\alpha$ emission extending along $\text{PA} = 45^\circ$. R98 suggest that the emission is reminiscent of a jet. A further 6 arcmin to the north-east, HH 406 is a large diffuse object. Are HH 405 and 406 related to HH 403/404? The IVN image (Fig. 19b) shows a reddened source (denoted HH 405IRS) at the position of HH 405. A reflection nebulosity is also seen nearby. The position of the

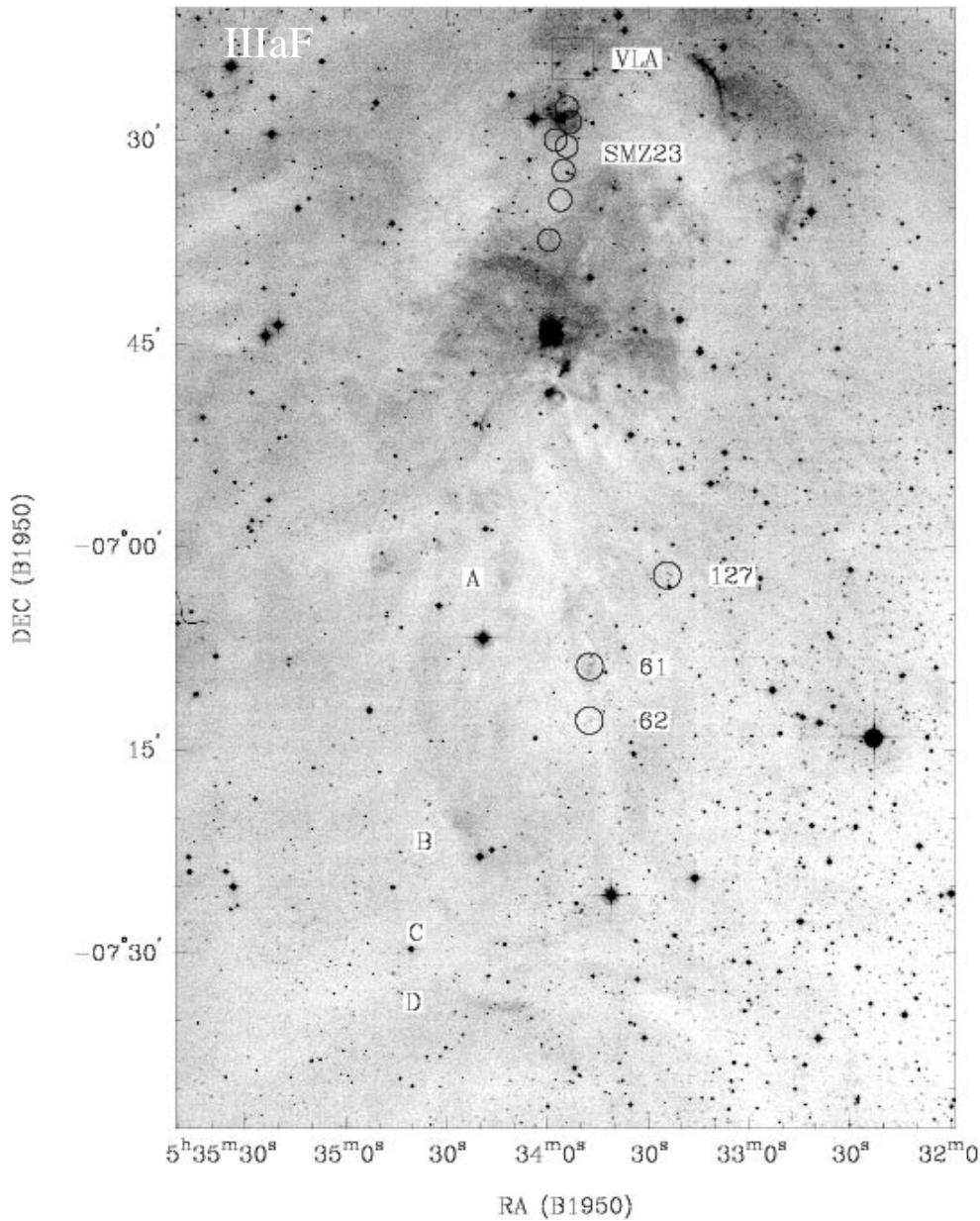


Figure 18. IIIaF image of features A, B, C and D to the far south of L1641-N. To the south-west the cloud boundary is clearly seen with respect to the background star field. The features are not visible on IIIaJ and IVN plates, which suggests that they are emission-line objects, possibly HH objects originating from the L1641-N region. The position of the VLA source is marked by a box for reference and comparison with Fig. 6. The near-infrared counterlobe to HH 306–310, SMZ 23, is indicated by open circles. HH 61/62 are thought to be associated with HH 303, while HH 127 represents a possible counterlobe to HH 403/404 (R98).

nearest *IRAS* source, 05347 – 0545, is shown in our IVN image. It is a 60- and 100- μm source only, indicating that it is heavily obscured and may be related to HH 405 and/or HH 406. Based on the location of HH 405IRS with respect to HH 405/406 and the reflection nebulosity, we suggest that this source is the driving agent for HH 405 and 406, thereby making the flow 0.78 pc in extent. Near-infrared polarimetry and imaging will be useful for determining if HH 405IRS or *IRAS* 05347 – 0545 is the illuminator of the reflection emission.

Located to the far south-west of L1641-N, R98 noted that HH 127 mirrors the position of HH 404 with L1641-N positioned at the centre (see Fig. 18). Although HH 127 lies at an angle of 10° from the HH 403/404 and L1641-N axis, they suggest that

HH 403/404 and 127 represent the blue- and redshifted lobes respectively of a 10.6-pc-scale flow centred on the VLA source. Given the clustered nature of potential outflow sources about the VLA source, proper motion studies of HH 127 and 403/404 are highly desirable to constrain the location of their energy source(s).

3.2.8 HH 407 (Figs 6, 13 and 20)

Located 28.3 arcmin north-west of L1641-N and within close proximity to HH 306–310, Figs 6 and 13 identify a large, highly fragmented structure located in the direction of several bright stars. The $H\alpha + [S\text{II}]$ image (Fig. 20) confirms it as a bona fide

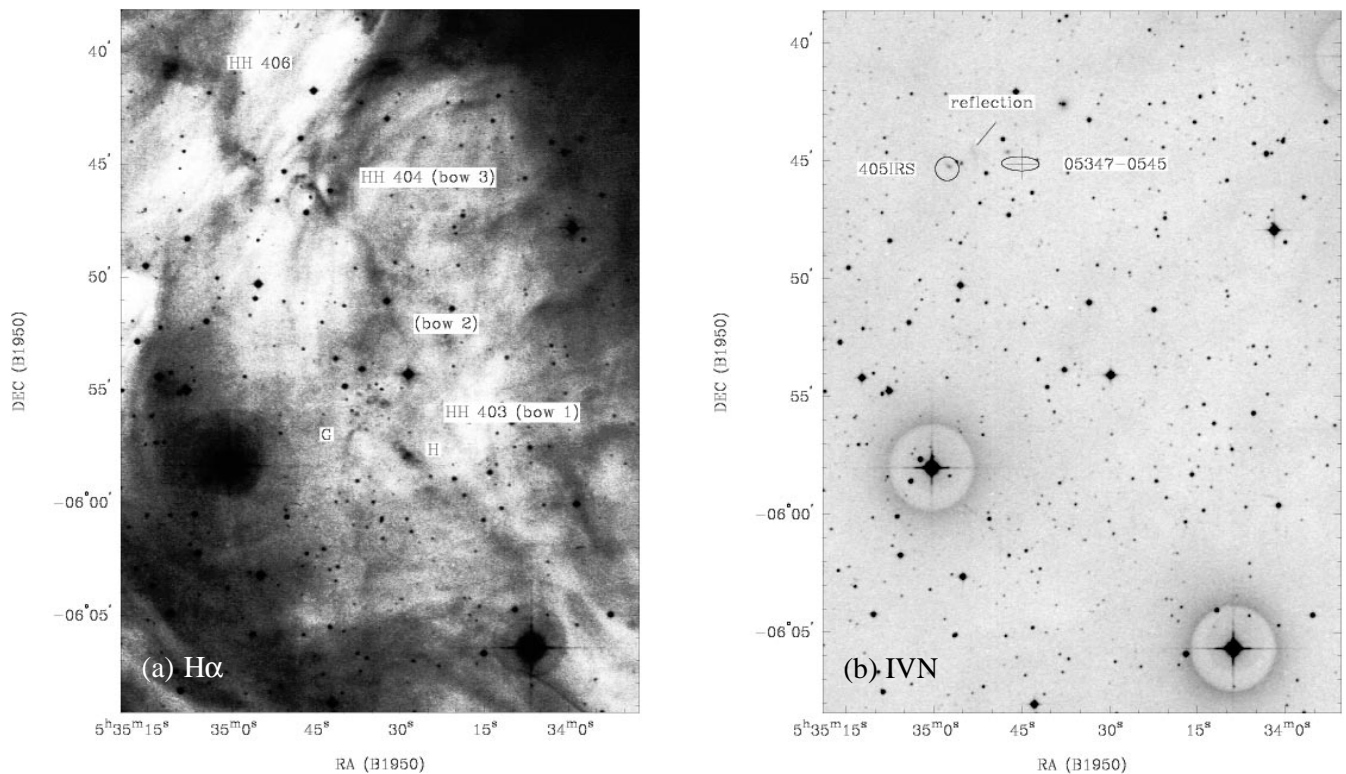


Figure 19. Scanned (a) $H\alpha$ and (b) IVN images of the HH 403/404 and 405/406 complexes identified in Fig. 6. The $H\alpha$ image has been enhanced so as to show that the HH 403/404 outflow has cleared away a significant portion of dust as it propagates away from the L1641-N region. HH 403/404 are located at the apexes of two large bow shocks (bow 1 and bow 3 respectively). The IVN image identifies a reddened source with associated reflection nebosity at the position of HH 405, which is the proposed energy source for HH 405/406. The nearby *IRAS* source 05347 – 0545 (labelled as 05347) may be related to HH 405/406 and/or the reflection nebosity between it and HH 405IRS. The major and minor axes of the *IRAS* error ellipse have been multiplied by 2 for clarity.

HH object as it emits predominately in [S II]. Knots A and B display bow shock structures with a streamer (knots C/D) extending to the south-east. In Figs 6 and 13, fainter $H\alpha$ emission extends a further 6 arcmin to the south-east of knots C/D.

As the streamers of HH 407 point towards the L1641-N region, it seems probable that the energy source lies in that direction. An examination of the H_2 data of SMZ98 does not reveal any emission extended towards HH 407. After re-examining our $H\alpha$ plate, we noticed the presence of a large loop-like structure (hereafter loop A) extending out of the reflection nebosity NGC 1999 and in the direction of HH 407. Comparison of our scanned $H\alpha$, IIIaF and IVN images (Fig. 21) indicates that loop A is a pure emission-line feature. Although faintly seen on the IIIaF image, the scanned $H\alpha$ image clearly distinguishes loop A from background emission.

In a recent study of the NGC 1999 region, Corcoran & Ray (1995, hereafter CR95) discovered a second loop (hereafter loop B) of $H\alpha$ emission extending west of the NGC 1999, which delineates a poorly collimated outflow associated with HH 35 and represents the counterflow to the redshifted molecular CO outflow discovered by Levreault (1988a,b). CR95 suggest that the Herbig Ae/Be star V380 Ori (which illuminates NGC 1999) drives HH 35, loop B and the molecular outflow. The presence of loops A and B suggests the presence of a quadrupole outflow in NGC 1999. Using similar arguments to CR95, we suggest that loop A delineates an optical outflow which, in conjunction with HH 407, represents a 6.2-pc lobe at $PA = -23^\circ$ with respect to V380 Ori.

In a search for optical counterparts to HH 407, our deep IIIaF plates do not reveal any clear candidates, although, if we assume

that loop A and HH 407 are propagating out and away from L1641, the southern counterflow may not yet have emerged from the far side of the molecular cloud. Stanke (private communication) has identified a large H_2 feature to the south of NGC 1999 which may represent an embedded counterflow to loop A and HH 407 (see Fig. 17). HH 130 is a large bow shock structure located 8.5 arcmin south-east of NGC 1999 and has been linked to HH 1/2 (Ogura & Walsh 1992) and V380 Ori (Reipurth, in preparation). CR95 suggest that the energy source of HH 130 is located to the north-east of knot H (see Fig. 21). If HH 130 and/or the H_2 feature represented the counterflow to loop A and HH 407, the outflow axis would be bent by up to 10° . A similar situation is seen in HH 127/403/404 (R98), HH 110/270 (Reipurth, Raga & Heathcote 1996) and HH 135/136 (Ogura et al. 1998). Proper motion and spectroscopic studies of HH 130, HH 407 and the H_2 feature are needed to determine if their motion and radial velocities are directed away from the V380 Ori region.

Is V380 Ori the driving source of loop A? In addition to V380 Ori, CR95 found two *K*-band sources, V380 Ori-B and V380 Ori-C, within NGC 1999. By means of speckle interferometry, Leinert, Richichi & Hass (1997) identified V380 Ori as a binary consisting of a Herbig Ae/Be (V380 Ori) and a T Tauri star. High-resolution millimetre interferometry of NGC 1999 will help to clarify which source is driving the optical emission associated with loop A.

As shown in Fig. 17, HH 306–310, HH 407 and the J -shaped filament (Bally et al. 1987; Johnstone & Bally 1999) lie within the rim of $H\alpha$ emission identified in Figs 6 and 13. Approximated by an ellipse $13.6 \times 4 \text{ arcmin}^2$ ($3.6 \times 0.54 \text{ pc}^2$) in size, we suggest that the ellipse has formed as a result of the combined action of

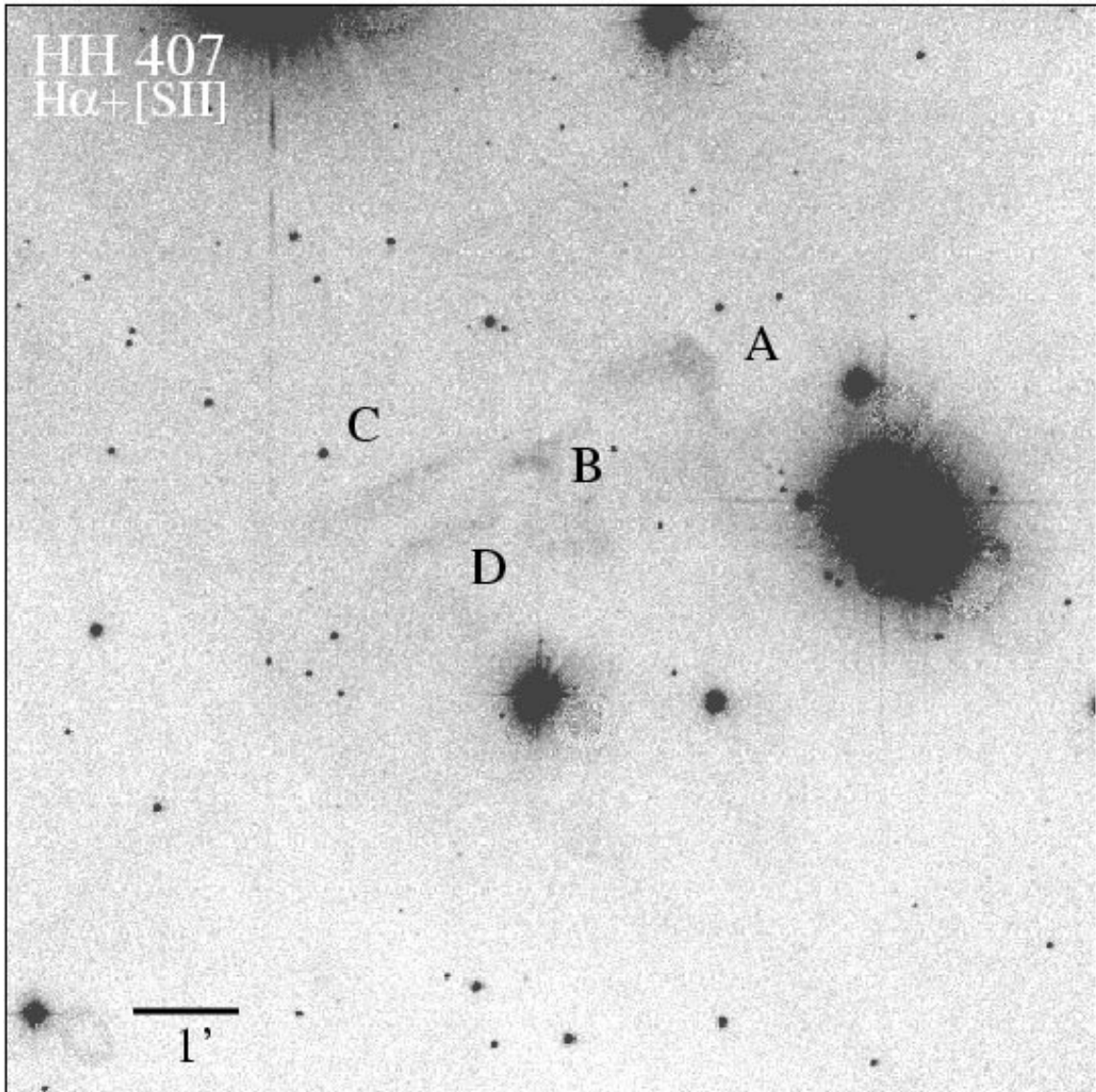


Figure 20. $H\alpha + [S II]$ image of the fragmented HH 407 bow shock identified in Figs 6 and 13. Knots A and B display arcuate morphologies. Objects C and D are part of a streamer which trails several arcminutes to the south-east.

the HH 306–310 and 407 flows expelling molecular gas from the main cloud core. The UV radiation from the nearby bright stars excites the outer edge of the expanding molecular material which we see as the $H\alpha$ ellipse. Such a large-scale movement of molecular gas by parsec-scale HH flows has been suggested for HH 34 and 306–310 (Bally & Devine 1994; R98).

4 CONCLUSIONS AND FUTURE WORK

By use of a single AAO/UKST $H\alpha$ film of the Orion region, we have identified emission-line nebulosities which resemble bow shocks, jets and extensive alignments of arc-shaped nebulae indicating possible giant molecular flows. Subsequent narrow- and broad-band CCD imaging has confirmed these features as genuine HH objects, tracing outflows ranging in size from a fraction of a parsec to over 6 pc in length. In addition to the 3-pc-wide $H\alpha$ rim surrounding HH 306–310 and 407, the $H\alpha$ loop (loop A)

extending out of the NGC 1999 reflection nebulosity have not been identified in previous studies. Although these features are faintly visible in our IIIaF images, the excellent contrast of the $H\alpha$ films with respect to IIIaF and published CCD images of these regions clearly distinguishes these features from background emission, thereby allowing a thorough investigation of how outflows from young stars affect the surrounding interstellar medium. The lack of optical and molecular emission associated with HH 403/404, the presence of the $H\alpha$ rim and the identification of large ^{13}CO cavities associated with HH 34 (Bally & Devine 1994), HH 306–310 (R98) and the SMZ 23 counterflow (this paper) suggest that, in the absence of massive star formation, parsec-scale flows are the dominating factor in disrupting molecular gas in GMCs. They may also be responsible for the continuation of star formation beyond the current epoch. The creation of large-scale cavities seen in ^{13}CO maps (R98; this paper) may produce highly compressed regions which collapse to form a new wave of star formation. In order to test this idea,

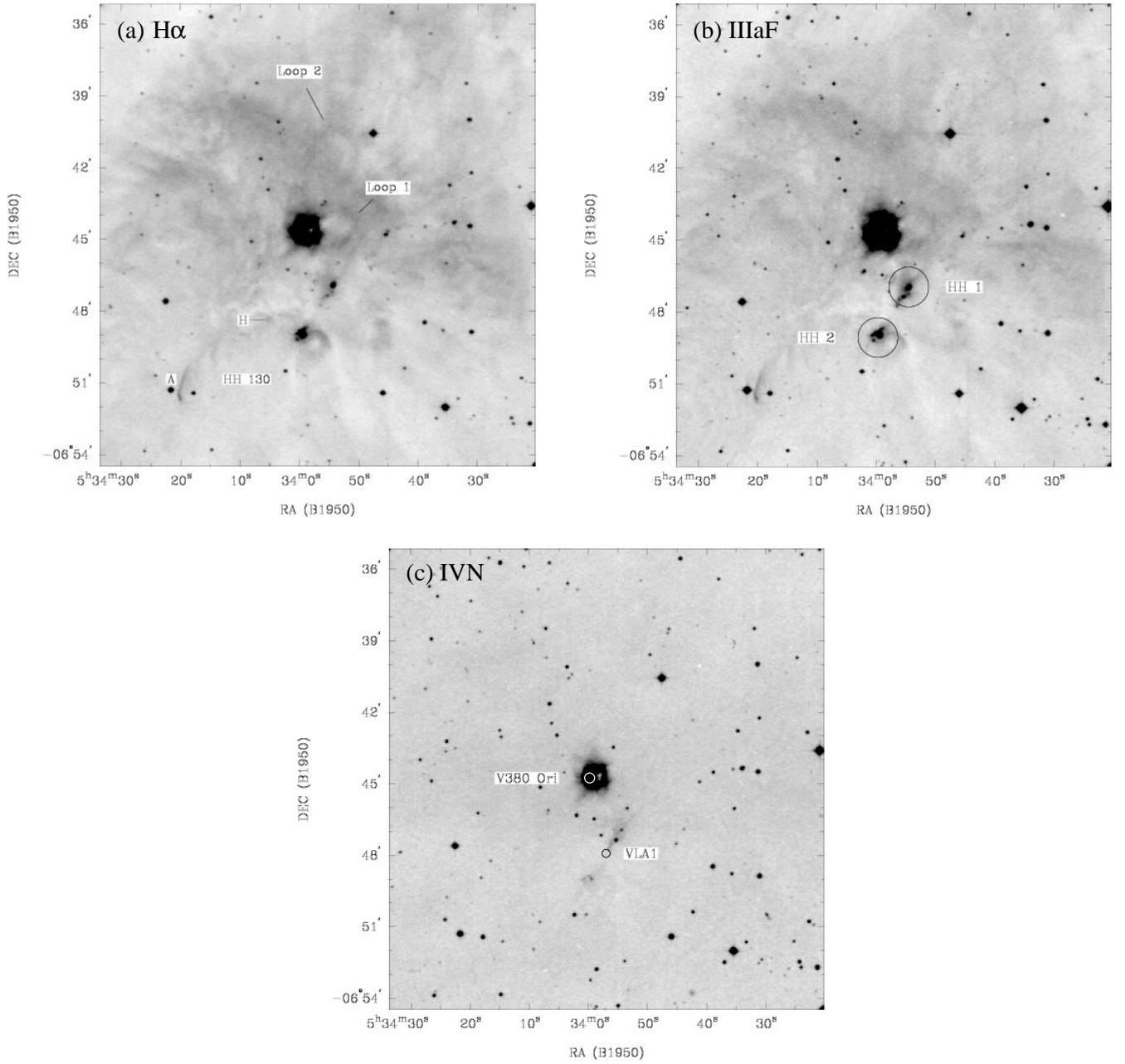


Figure 21. Scanned (a) H α , (b) IIIaF and (c) IVN images of the NGC 1999 region. The H α image clearly identifies two loops of emission extending out of NGC 1999. HH 130 is a large arcuate object which extends from the bright bow shock HH 130A to HH 130H. The IVN image indicates the positions of V380 Ori and VLA1, which are the illuminating and driving sources of NGC 1999 and HH 1/2 respectively.

high-resolution submillimetre observations in conjunction with near-infrared H $_2$ (2.12 μ m) imaging will identify and determine the distribution of newly forming Class 0 protostars with respect to the CO cavities.

Although we have suggested candidate energy sources for many of the new HH flows, only a few (Ori I-2, BE Ori and V510 Ori) can be considered as certain. The identification of at least four sources within an arcminute of the VLA source warrants subarcsecond CO mapping of the region to determine which source is driving the optical and near-infrared emission associated with HH 306–310, HH 403/404, HH 407 and SMZ 23. Near-infrared spectroscopy of proposed outflow sources for HH 298/301/302, 304, 305 and 405 will be useful in classifying their

nature for comparison with other HH energy sources. To varying degrees, the optical sources BE Ori and V510 Ori exhibit optical variability and multiple-ejection events (HH objects). The fact that these sources still possess highly collimated, one-sided jets well after they have emerged from their parental molecular cloud may provide important insights into jet evolution.

In relation to the newly discovered parsec-scale flows, high-resolution spectroscopy and proper motion studies of individual knots associated with HH 61/62/303, HH 306–310, HH 127/403/404, HH 407 and features A–D to the far south of L1641-N will determine velocities and excitation conditions, and confirm points of origin.

Owing to the success of the Orion H α film, the Carina, Cha I/II,

SCO OB1, ρ Oph, R Cra and CMa OB1 SFRs are to be surveyed in a similar fashion to that presented in this paper. The majority of these cloud complexes lie within 500 pc and maximize the detection of faint, large-scale flows for comparative studies with the Orion region, where we hope to address the following questions.

(i) What is the nature of the energy source? Parsec-scale flows are associated with class 0, class I and optically visible T Tauri stars. Is the parsec-scale phenomenon a result of inherent properties of the energy source?

(ii) How does the flow remain collimated over such large distances? Does the nature of the surrounding environment have a collimating effect?

(iii) To what extent do parsec-scale outflows affect star formation within molecular clouds? Is there any evidence for self-regulated star formation?

ACKNOWLEDGMENTS

We thank the staff of the AAO and particularly the UKST for the teamwork which makes the $H\alpha$ survey possible. Thanks also go to the Mount Stromlo Time Allocation Committee for the generous allocation of time on the 40-inch telescope. SLM acknowledges John Bally for the use of the Bell Labs 7-m ^{13}CO data, and Thomas Stanke for supplying his H_2 data of the L1641-N region. Thanks also go to David Malin at the AAO for providing unsharp-mask prints of the Orion film. SLM acknowledges the support of a DEET scholarship and an Australian Postgraduate Award. We thank the anonymous referee for comments and suggestions which strengthened the paper. This research has made use of the SIMBAD data base, operated at CDS, Strasbourg, France, and the ESO/SERC Sky Surveys, based on photographic data obtained using the UKST which is currently operated by the AAO. IRAF is distributed by the National Optical Astronomy Observatories, which are operated by the Association of Universities for Research in Astronomy, Inc., under cooperative agreement with the National Science Foundation.

REFERENCES

Anglada G., Villuendas E., Estalella R., Beltrán M. T., Rodríguez L. F., Torrelles J. M., Curiel S., 1998, *AJ*, 116, 2953
 Bally J., Devine D., 1994, *ApJ*, 428, L65
 Bally J., Stark A. A., Wilson R. W., Langer W. D., 1987, *ApJ*, 312, L45
 Bally J., Devine D., Reipurth B., 1996, *ApJ*, 473, L49
 Brown A. G. A., De Geus J., De Zeeuw P. T., 1994, *A&A*, 289, 101
 Cernicharo J., Bachiller R., Duvert G., Gonzalez-Alfonso E., Gomez-Gonzalez J., 1992, *A&A*, 261, 589
 Chen H., Tokunaga A. T., Strom K. M., Hodapp K.-W., 1993, *ApJ*, 408, 646
 Chen H., Zhao J.-H., Ohashi N., 1995, *ApJ*, 450, L71
 Codella C., Palumbo G. G. C., Pareschi G., Scappini F., Caselli P., Attolini M. R., 1995, *MNRAS*, 276, 57
 Cohen M., Kuhl L. V., 1979, *ApJS*, 41, 743
 Corcoran D., Ray T. P., 1995, *A&A*, 301, 729 (CR95)
 Davis C. J., Eislöffel J., 1995, *A&A*, 300, 851 (DE95)

Davis C. J., Mundt R., Eislöffel J., Ray T. P., 1995, *AJ*, 110, 766
 Devine D., Bally J., Reipurth B., Heathcote S., 1997, *AJ*, 114, 2095
 Eislöffel J., Mundt R., 1997, *AJ*, 114, 280
 Foster P. N., Boss A. P., 1996, *ApJ*, 468, 784
 Fukui Y., Sugitani K., Takaba H., Iwata T., Mizuno A., Ogawa H., Kawabaa K., 1986, *ApJ*, 311, L85
 Fukui Y., Takaba H., Iwata T., Mizuno A., 1988, *ApJ*, 325, L13
 Gum C. S., 1955, *Mem. R. Astron. Soc.*, 67, 155
 Heathcote S., Morse J. A., Hartigan P., Reipurth B., Schwartz R. D., Bally J., Stone J. M., 1996, *AJ*, 112, 1141
 Hirth G. A., Mundt R., Solf J., 1997, *A&AS*, 126, 437
 Hodapp K., 1994, *ApJS*, 94, 615
 Hodapp K.-W., Deane J., 1993, *ApJS*, 88, 119
 Jankovics I., Appenzeller I., Krautter J., 1983, *PASP*, 95, 883
 Johnstone D., Bally J., 1999, *ApJ*, 510, L49
 Leinert C., Richichi A., Hass M., 1997, *A&A*, 318, L472
 Levreault R. M., 1988a, *ApJS*, 67, 283
 Levreault R. M., 1988b, *ApJ*, 300, 897
 López R. et al., 1998, *AJ*, 116, 845
 Magazzu A., Martin E. L., 1994, *A&A*, 287, 571
 Malin D. F., Ogura K., Walsh J. R., 1987, *MNRAS*, 227, 361
 Miller L., Cormack W., Paterson M., Beard S., Lawrence L., 1992, in MacGillivray H. T., Thomson E. B., eds, *Digitised Optical Sky Surveys*. Kluwer, Dordrecht, p. 133
 Mundt R., 1988, in Dupree A. K., Lago M.T.V.T., eds, *Formation and Evolution of Low Mass Stars*. Kluwer, Dordrecht, p. 257
 Mundt R., Bastian U., 1980, *A&AS*, 39, 245
 Ogura K., Walsh J. R., 1991, *AJ*, 101, 185
 Ogura K., Walsh J. R., 1992, *ApJ*, 400, 248
 Ogura K., Sugitani K., 1998, *Proc. Astron. Soc. Aust.*, 15, 91
 Ogura K., Kakano M., Sugitani K., Liljeström T., 1998, *A&A*, 338, 576
 Parker Q. A., Bland-Hawthorn J., 1998, *Proc. Astron. Soc. Aust.*, 15, 33
 Parker Q. A., Phillipps S., 1998a, *Proc. Astron. Soc. Aust.*, 15, 28
 Parker Q. A., Phillipps S., 1998b, *Astron. Geophys.*, 39, 10
 Parker Q. A., Phillipps S., Morgan D. H., 1995, in Chapman J., Cannon R. D., Harrison S., Hidayat B., eds, *Proc. IAU Colloq. 148, ASP Conf. Ser. Vol. 84, The future utilisation of Schmidt telescopes*. Astron. Soc. Pac., San Francisco, p. 96
 Reipurth B., 1985, *A&AS*, 61, 319
 Reipurth B., Graham J. A., 1988, *A&A*, 202, 219
 Reipurth B., Raga A. C., Heathcote S., 1996, *A&A*, 311, 989
 Reipurth B., Bally J., Devine D., 1997, *AJ*, 114, 2708
 Reipurth B., Devine D., Bally J., 1998, *AJ*, 116, 1396(R98)
 Rodgers A. W., Campbell C. T., Whiteoak J. B., 1960, *MNRAS*, 121, 103
 Rodríguez L. F., Reipurth B., 1994, *A&A*, 281, 882
 Sanduleak N., 1971, *PASP*, 83, 95
 Stanke T., McCaughrean M. J., Zinnecker H., 1998, *A&A*, 332, 307 (SMZ98)
 Strom K. M., Margulis M., Strom S. E., 1989a, *ApJ*, 346, L33
 Strom K. M., Margulis M., Strom S. E., 1989b, *ApJ*, 345, L79
 Strom K. M. et al., 1990, *ApJ*, 362, 168
 Sugitani K., Fukui Y., Mizuni A., Ohashi N., 1989, *ApJ*, 342, L87
 Wiramihardja S. D., Kogure T., Yoshida S., Nagano M., Ogura K., Iwata T., 1991, *PASJ*, 43, 27
 Woitas J., Leinert C. H., 1998, *A&A*, 338, 122
 Wouterlout J. G. A., Walmsley C. M., 1986, *A&A*, 168, 237
 Yun K., Bally J., Devine D., 1997, *ApJ*, 485, L45
 Zealey W. J., Mader S. L., 1997, *Proc. Astron. Soc. Aust.*, 14, 200

This paper has been typeset from a \TeX/L\TeX file prepared by the author.